



**POLITECNICO**  
MILANO 1863

SCUOLA DI INGEGNERIA INDUSTRIALE  
E DELL'INFORMAZIONE

# Self-consumption photovoltaic plant: Project Verdeto 127,68kWp

TESI DI LAUREA MAGISTRALE IN  
ELECTRICAL ENGINEERING  
INGEGNERIA ELETTRICA

Author: **Nicolò Meo**

Student ID: 10574158

Advisor: Dario Zaninelli

Co-advisor: Michela Longo

Academic Year: 2022/2023



## Abstract

The analysis of grid-connected industrial PV systems is the focus of this paper. In particular, the first chapter describes the state of the art of photovoltaic systems and thoroughly examines each of its constituent parts. Thus, the characteristics of solar energy and solar irradiation are examined before we get into the specifics of how the systems for converting solar energy into electricity are designed and operated. Then, a description of the development and technology of photovoltaic modules follows. Investigating the first, second, and third generations of photovoltaic modules in detail follows an examination of their composition and operation, which results in the characteristic curves. The analysis of conversion devices follows, first outlining the fundamental principles and traits of inverters, then looking into the various configurations that are possible. The primary characteristics of AC cables and DC cables are then looked at in relation to the topic of solar cables. The interface with the medium-voltage power distributor and consequently the necessary devices, such as the general device, the interface protection device, and finally the generator device, are thoroughly investigated to bring the state of the art to a close. The study case, the Verdeto photovoltaic power plant, with a peak power of 128.68kW, is the focus of the second chapter. An overview of the subject of grid-connected plants, also known as self-consumption power plants, is provided before delving into the specifics of Italian regulation for plants of this kind. The focus then shifts to the extent of the work completed at STEAG Sens Srl. I'll start with the feasibility study. Thus, the study of the plant's location, solar radiation, and ultimately the load analysis. The modules, substructures, inverters, and cables that were important for the sizing process used during the design of the Verdeto photovoltaic system are then thoroughly examined. The second section describes in detail the outcomes of the simulations that were performed as part of the preliminary stage and were necessary for the client presentation of the project. Sunny Design and PVSyst are the two tools used specifically. Investigating the differences between the two software, these subchapters also highlight the reasons for the discrepancies between the two simulations. The results of PVSyst, the more precise and trustworthy software, are compared with data extrapolated from the POD present on the Verdeto power plant to conclude the technical analysis chapter. The project's economic analysis is then

made, highlighting the project management and business plan phases and looking into the key performance indicators.



# Contents

<b>Abstract</b> .....	<b>iii</b>
<b>Contents</b> .....	<b>vi</b>
<b>1 State of Art: Photovoltaic Power Plant</b> .....	<b>9</b>
1.1. Operating Principle of Photovoltaic Systems.....	9
1.1.1. Solar Energy and Solar Irradiance.....	9
1.1.2. Conversion Devices: Cells Operating Principles and Structure .....	14
1.2. Modules History and Technology .....	20
1.2.1. Photovoltaic Modules Composition .....	21
1.2.2. Photovoltaic Module Characteristic Curves.....	23
1.2.3. First Photovoltaic Modules Generation.....	26
1.2.4. Second Photovoltaic Modules Generation.....	26
1.2.5. Third Photovoltaic Modules Generation.....	30
1.3. Inverters Technology and Configuration .....	31
1.3.1. Inverters General Characteristics .....	31
1.3.2. Conversion Unit Configurations .....	35
1.4. Solar Cables Characteristics .....	38
1.4.1. AC Cables Analysis .....	38
1.4.2. DC Cables Analysis .....	39
1.5. Interface to MT Distribution Network .....	42
1.5.1. General Devices Characteristics (DG) .....	44
1.5.2. Interface Protection Devices Characteristics (DDI) .....	44
1.5.3. Generator Devices Characteristics (DDG) .....	45
<b>2 Case of Study</b> .....	<b>47</b>
2.1. Introduction: Self-consumption Photovoltaic Power Plant .....	47
2.2. Photovoltaic power plant: Project Verdeto 127.68kWp .....	49
2.2.1. Feasibility Analysis.....	49
2.2.1.1. Location Analysis.....	49
2.2.1.2. Irradiation Analysis .....	52
2.2.1.3. Load Analysis .....	53

2.2.2.	Technical Analysis of Verdeto photovoltaic plant.....	56
2.2.2.1.	Modules and Substructures: generalities & technical analysis	56
2.2.2.2.	Inverters: generalities and technical analysis .....	62
2.2.2.3.	Cables: generalities & technical analysis .....	65
2.2.3.	Productivity Simulation .....	67
2.2.3.1.	SunnyDesign Software Productivity Simulation .....	67
2.2.3.2.	PVsyst software productivity simulation.....	73
2.2.4.	Results comparison .....	82
<b>3</b>	<b>Economic Overview .....</b>	<b>85</b>
3.1.	Economic Computation.....	85
3.2.	Project management.....	90
	<b>Conclusions.....</b>	<b>95</b>
	<b>Bibliography.....</b>	<b>99</b>
	<b>List of Figures.....</b>	<b>101</b>
	<b>List if Tables .....</b>	<b>105</b>





# 1 State of Art: Photovoltaic Power Plant

## 1.1. Operating Principle of Photovoltaic Systems

### 1.1.1. Solar Energy and Solar Irradiance

Our planet warming derives from solar energy. Nuclear fusion reactions take place inside the sun's core, transforming mass into energy. Among these, the one that fuses hydrogen atoms and creates helium atoms, releasing energy.

This energy is transmitted from the innermost to the outermost layers by conduction, convection and irradiation.

The majority part of the energy that is radiated by the sun towards the earth is transported as electromagnetic waves (photons) which are generated permanently by the sun. About 70% of this energy passes through the atmosphere, while the other portion goes back by reflection. The radiation that passes through gets diffuses by the atmosphere, another part is reflected or absorbed by the ground as is shown in Figure 1.

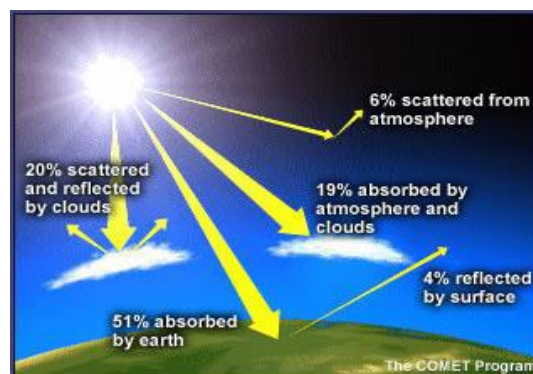


Figure 1: Sun's Energy Distribution

The irradiance is the magnitude for describing the incident power per the surface unit by the electromagnetic radiation that comes from the sun. This value corresponds to the integral of the power associated to each value of the solar radiation spectrum frequencies, and its unit is  $\left[\frac{kW}{m^2}\right]$ .

The photosphere is the outer layer of the convective zone, and the total solar irradiance is approximately  $63 \frac{kW}{m^2}$ ; this value decreases geometrically with the increasing of sun distance until the outer zone of the atmosphere is reached, where the total solar power is  $1367 \frac{W}{m^2}$ , defined as solar constant. Since the distance between the Earth and the sun varies during the year, the solar constant represents the mean value of the specific power, it varies in an interval of  $\pm 3\%$ .

Furthermore, the rotational axis of the earth is not perpendicular the plane of revolution, but it is inclined by  $23,45^\circ$ . In light of this, the two hemispheres are irradiated in different manners depending on the month considered, as is shown in figure 2.

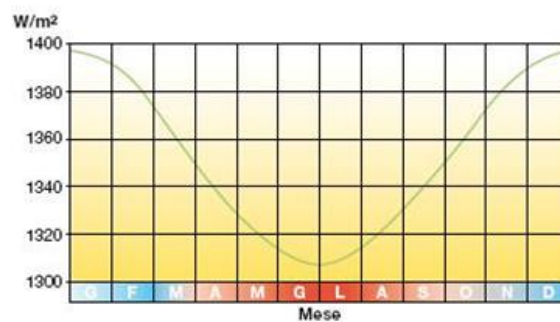


Figura 2: Extra-terrestrial Solar Radiation

The solar radiation is the integral of the irradiance over a specified space of time; its unit is  $[\frac{kWh}{m^2}]$  and can reach the soil directly or diffusely.

Regarding the solar radiation, the maximum of the spectral distribution is situated in the area of visible light (with a wavelength between  $0.38\mu m$  and  $0.78 \mu m$ ) and drop down going to the ultraviolet radiation (UV:  $0.2 \mu m$ -  $0.38 \mu m$ ) and the infrared radiation (IR:  $0.79 \mu m$ - $2.6 \mu m$ ) as is shown in Figure 1.3.

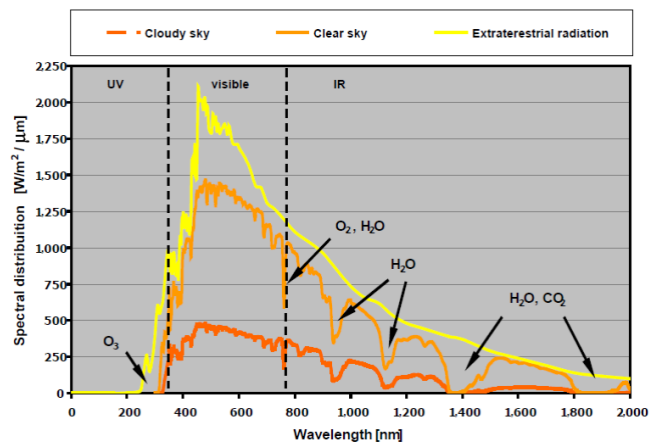


Figura 3: Spectrum of Solar Radiation

The main aspects that affect solar radiation are:

- Sun elevation: the amount of solar radiation reaching the surface is highly dependent on the elevation of the sun. In tropical regions where the sun is nearly vertical in the summer UV levels are high. By contrast, in the polar regions of the sun elevation is low even in summer, consequently mean solar radiation levels are low or moderate. This phenomenon is shown in Figure 4.

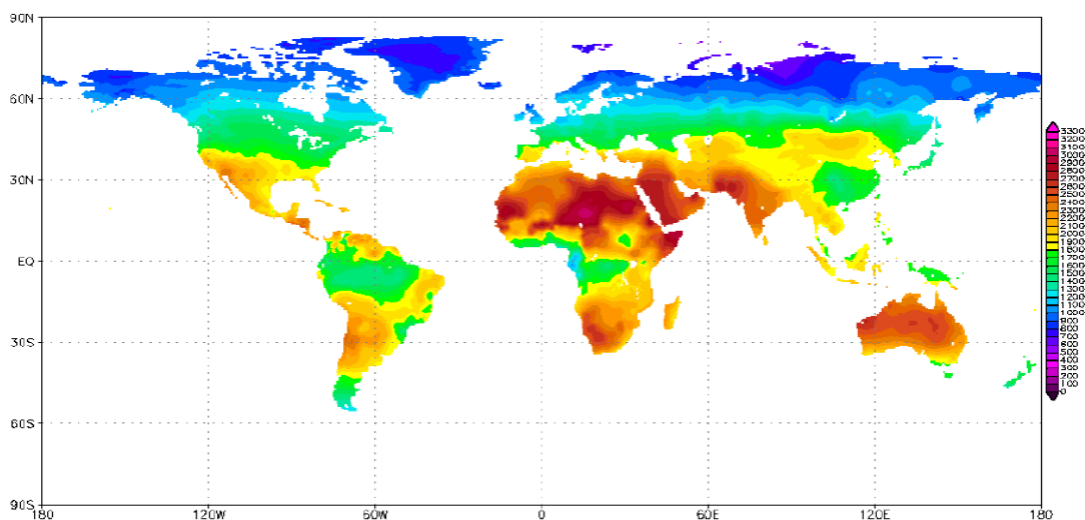


Figura 4: Global Solar Radiation

- Cloudiness: clouds have an important effect in the radiation effect, the fraction of the sky covered by clouds affect the intensity and spectral composition of the

radiation that actually reaches the Earth surface. The amount of radiation attenuated by the cloud will be according to the type of cloud and its density, as it is expected the denser and darker is the cloud the sunbeam blocking effect will be higher.

- Zenith angle ( $h$ ): this angle depends on the time of the day, season, and latitude of the place. The influence of this factor has two aspects, one purely geometric, since the radiation flux passing through the atmosphere varies with the orientation of the surface: if it is parallel to the radiation of incidence, the solar radiation is zero, while if it is perpendicular, is maximum. In addition to this effect, increasing zenith angle implies that radiation must traverse a thicker atmospheric layer, and therefore its attenuation is increased.
- Length of the path: this factor depends on the latitude and day of the year. When the sun is near the horizon, the radiation travels a long path through the atmosphere, as a consequence less UV rays reach the surface of the earth.

The precedent analysis leads to understand that, at the soil level, the total specific energy is less than the solar constant, due to the absorption and to the diffusion phenomenon that happens in the atmosphere.

Therefore, it has been defined the  $AM$  (air mass) index by (1), which expresses the relative quantity of atmosphere that the sun's rays pass through before reaching the ground. In Equation (1),  $h$  is the zenith angle as it was explained previously.

$$AM = \frac{1}{\sin h} \tag{1}$$

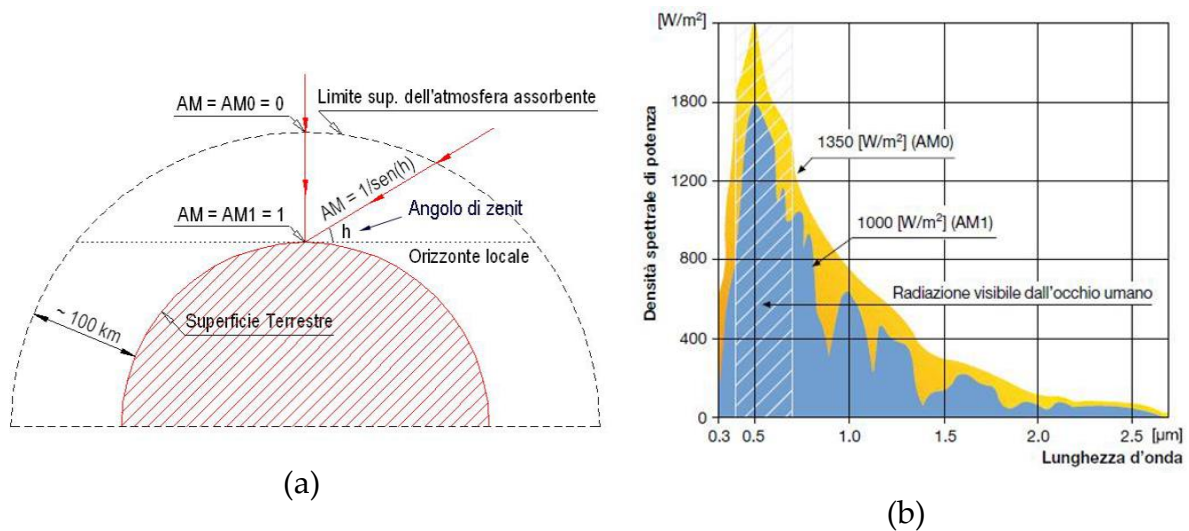


Figura 5: (a) Air Mass Definition, (b) Spectral Power Density

Considering Figure 1.5 (a), AM0 spectrum represents the absence of the atmosphere and AM1 indicates the standard atmosphere thickness crossed by the sun's rays in a direction perpendicular to the earth's surface and measured at sea level.

For completeness, Figure 1.5 (b) shows the variation of the power spectral density as a function of different AM.

As a result of the previous analysis, the maximum radiation falling on the earth's surface at midday is  $1000 \frac{W}{m^2}$  when the sky is cloudless.

This so-called global radiation is composed of direct radiation, diffuse radiation and albedo radiation as shown in Figure 6.

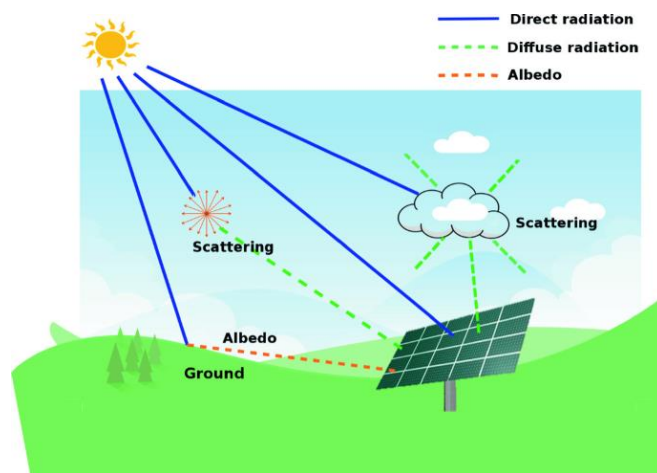


Figura 6: Solar Radiation Composition

- Direct (or Beam) radiation: it comes directly from the sun without change of direction.
- Diffuse radiation: it is the result of the scattering of the sunbeam or reducing the magnitude of the sunbeam due to the atmospheric constituents, as previously explained.
- Albedo radiation: it is the reflection due to the ground or the surrounding environment.

Each material has an albedo coefficient, and it describes its capacity to reflect the light. In Table 1.1 the most useful Albedo coefficient are reported. [1], [2], [3], [4], [5]

Tabella 1: Albedo Coefficients

Location	Albedo [%]
Ocean	2 - 10
Forest	6 - 18
Grass	7 - 25
Soil	10 - 20
Desert (land)	35 - 45
Ice	20 - 70
Snow (fresh)	70 - 80

### 1.1.2. Conversion Devices: Cells Operating Principles and Structure

The photovoltaic cell is composed by semiconductor material, usually crystal silicon, since nowadays it has the more efficient cost/watt rate. Its thickness is a few hundred of micromillimeters and it is equipped with two contacts: a front metal grille and a rear metal plat for the collection of the electric energy.

When the cell is exposed to the sun light, it is able to convert partially the energy of the photons, thanks to the interaction between these photons and the valence electrons of the silicon lattice.

Each atom of the silicon crystal lattice is surrounded by four others in which each of them shares one of its four valence electrons, belonging to the outermost orbits, forming a covalent bond. In this way it is possible to complete the external octet and thus make the configuration stable. The silicon lattice is shown in Figure 7. The lattice is shown with square shape for on plane representation instead in reality the lattice takes the tetrahedral shape.

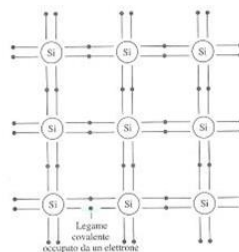


Figura 7: Silicon Crystal Lattice

The energy levels allowed to electrons, through quantum mechanics, are arranged in energy bands. The terms conduction band and valence band represent the portions of the energy band diagram where the energy levels allowed to the electrons are located.

$E_v$  represents the maximum energy value that an electron can assume in the valence band, while  $E_c$  represents the minimum value in the conduction band. An electron cannot have an energy value included in the bandgap  $E_g$ .

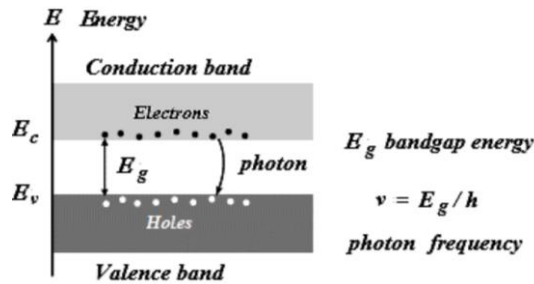


Figura 8: Energy Band Model

As it is shown in Figure 8, the difference  $E_g = E_c - E_v$  is the forbidden band, and it represents the minimum value of energy necessary to break a covalent bond and to free an electron.

In a pure crystal, called intrinsic, the electrons bound in the covalent bonds with other atoms, are in energetic state that belongs to the valence band, and they do not have the energy necessary to switch the conduction band. When a photon of suitable energy affects the semiconductor, it interacts with the electrons causing their excitation.

Denote with  $E_f = h \cdot v$  the energy of a photon, where  $h$  is the Plank constant and  $v$  is the frequency of the radiation. If the photon has got enough energy, thus  $E_f > E_g$ , therefore it is able to break the covalent bond and to excite an electron. The free electron passes from the valence band to the conduction band. For each electron that pass the band gap, a hole is formed in the valence band and therefore an electron-hole pair is generated. Using a pure single crystal, excitation is immediately followed by recombination, therefore the phenomenon is useless. [4]

The conductivity of silicon can be modified by means of doping process, in which atoms of impurities are inserted in the lattice.

In light of this, silicon atoms are replaced with atoms of the fifth group of the periodic table of elements (for example Phosphorous (P) or Arsenic (As)), which presents five electrons in the valence band. This leads to a surplus electron only loosely bound by the Coulomb Force, which can be ionized by a little amount of energy (0,002 eV). Since pentavalent elements easily donate an electron, they are called donor. The current transport in such a material practically occurs only by means of electrons, it is called n-type material.

In the other hand, if silicon atoms are replaced with trivalent element, such as Boron (B), aluminum (Al) or Gallium (Ga), leads to a lack of an electron. This means that an electron near a hole can fill up this blank and leaves a new hole at its original position consequently. This results in the current conduction by means of positive holes. Therefore, this material is called p-type material. Trivalent atoms, which easily accept an electron, are defined as acceptors.



Figure 9: (a) P-type Material Example, (b) N-type Material Example

By placing p-type silicon in contact with n-type silicon, a PN junction is created. Due to the diffusion phenomenon, one has that the gaps will diffuse from p-type to the n-type region, while the electron will diffuse from the n-type to the p-type region.

If this process continued undisturbed, there would eventually be a uniform concentration of charges in the semiconductor, and the PN junction would vanish. To balance the diffusion current, another process occurs, represented by a drift current. As the gaps diffuse from region p to region n, in the p region there are acceptor atoms negatively charged; Similarly, the electrons leave positively charged donor atoms in the n region. A spatially charged region is thus formed in the junction, full of stucked carriers. These concentration differences lead to the fact that electrons from the n-region diffuse into p-region and holes from the p-region diffuse into the n-region.

Diffusion currents of holes into the n-region result as a result. A deficit of charges forms inside the previously electrically neutral areas as a result of the movement of negative and positive charges. The donor region experiences a positive charge, whereas the acceptor region has a negative charge. As a result, an electrical field forms over the boundary surface and induces currents from both types of charge carriers that oppose diffusion currents. The total amount of current flowing across the boundary surface is zero in the equilibrium. The field currents entirely offset the diffusion currents, just as the hole and electron currents completely offset one another. This electrostatic force that extends beyond the boundary surface corresponds to the potential difference  $V_d$ , also known as diffusion voltage (in the order of 0,8eV). The charge carriers created by light in the solar cell are separated as a result of this electrical field. The so-called space-charge zone, which is where stationary electrical positive and negative charge exists, has a severe shortage of mobile charge carriers and a very



high impedance. The diffusion voltage, electrical field intensity, and therefore the field currents are all decreased when the n-region is applied with a negative voltage (forward bias). They no longer balance the electron and hole diffusion currents as they would have done in the absence of exogenous voltage. As a result, the p-n junction experiences a net diffusion current from electrons and holes. The current is only constrained by the bulk resistors if the applied voltage is equal to the diffusion voltage, which causes the field currents to vanish. On the other hand, a positive voltage supplied to the outside of the n-region (reverse bias) adds to the diffusion voltage, expands the space-charge zone, and ultimately overpowers the field current. The resultant current, whose reverse bias direction is opposite, is very weak. Graphic explanation of the phenomenon is shown in Figure 10.

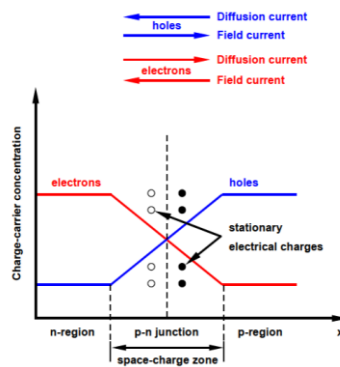


Figura 10: p-n Junction Graphic Explanation

Not all the solar radiation incident to the photovoltaic cell is usable in the conversion process. From the known equation  $E_f = h \cdot \nu$ , it is observable that the energy of the photon depends on the frequency of the radiation. Between frequency  $h$  and wavelength  $\lambda$ , the relation  $h = \frac{1}{\lambda}$  exists in the case of light radiation.

Considering silicon, the maximum wavelength is  $\lambda = 1.15\mu m$ . The fraction that exceeds this limit has insufficient energy and therefore cannot be used in the conversion process. Photons with energy more than the required constitute a surplus that must be dissipated in heat.

In Figure 11 a basic schematic image of a photovoltaic cell is shown.

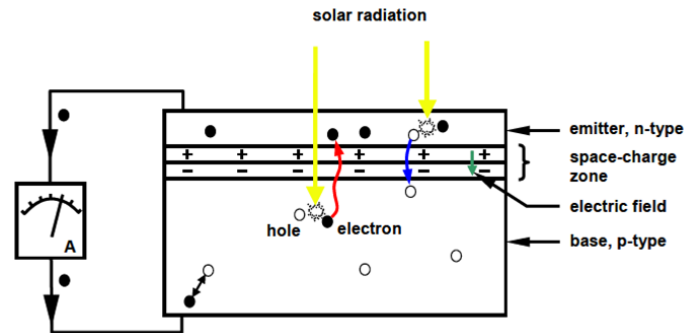


Figure 11: Basic Scheme of PV cell

Now that the background of cell operating principle was introduced, this chapter will assess the equivalent electric circuit and the characteristic curves of the PV cell. The electric equivalent circuit of a real PV cell is shown in Figure 11.

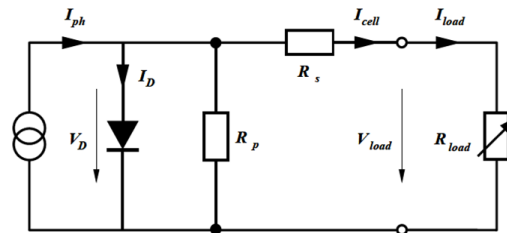


Figure 12: Equivalent Circuit of a PV Cell

The equivalent circuit is composed by:

- Photocurrent generator: the magnitude of the photocurrent generator depends on the radiation intensity; it is proportional to the irradiance.
- Diode: the diode is created by the p-n junction; in fact, the mathematical process at the p-n junction leads to the diode Equation (2)

$$I_d = I_0 \cdot \left[ e^{\frac{qV}{kT}} - 1 \right] \quad (2)$$

Where:  $I_d =$  Diode current [A]

$q =$  Magnitude of electron charge [ $1.6 \cdot 10^{-19}C$ ]

$V =$  Applied voltage [V]

$k =$  Boltzmann's constant [ $8,65 \cdot 10^{-5} \frac{eV}{K}$ ]

$T =$  Absolute temperature [K]

The quantity  $I_0$  defines the saturation current of a diode.

- $R_s$ : the series resistance arises from the bulk resistance of the silicon wafer, the resistance of the metallic contacts the front and back surface and further circuit resistances from connections and terminals.

The current  $I_{cell}$  is given by Equation (3).

$$I_{cell} = I_{ph} - I_0 \left( e^{\left( \frac{q(V_{load} + I_{cell} \cdot R_s)}{kT} \right)} - 1 \right) - \frac{V_{load} + I_{cell} \cdot R_s}{R_p} \quad (3)$$

The maximum value of current that can be delivered by a solar cell is denominated short circuit currents  $I_{sc}$  and is achieved when a zero-ohm load is connected to the output terminals of the cell ( $V=0$ ). This value depends on the surface of the panel and the solar radiation. On the other hand, when the load absorbs zero-current ( $I=0$ ) in the terminals of the cell it can be measured the open circuit voltage  $V_{oc}$ . The open circuit voltage and the short circuit current of the PV cell are expressed by Equation (5) and Equation (6).

$$V_{oc} = \frac{kT}{q} \cdot \ln \left( \frac{I_{ph}}{I_0} + 1 \right) \quad (5)$$

$$I_{sc} = I_0 \cdot e^{\left( \frac{qV_{oc}}{kT} \right)} \quad (6)$$

To asset the efficiency of a cell, it is tested under 'Standard Test Conditions' (STC), which implies irradiance of  $1000 \frac{W}{m^2}$ , a temperature of  $25^\circ C$  and an AM1.5 spectrum. The efficiency of the cell expresses the ability to convert solar energy into electrical and is defined as  $\eta = \frac{P_{stc}}{G \cdot A}$

where  $P_{stc}$  is the maximum power that can be produced in STC ( $W_{peak}$ ),  $G$  indicated the irradiance in STC and  $A$  the area of the cell.

A further merit factor is the fill factor, defined as:  $FF = \frac{V_{stc} \cdot I_{stc}}{V_{oc} \cdot I_{sc}}$ . The  $FF$  gives an indication of the quality of the cell. It indicates how far the  $I-V$  characteristic curve approximates to a rectangle. Normally the value for crystalline solar cell is about 0.7-0.8.

To conclude the paragraph, it is interesting to analyze the sources of losses in solar cell:

- The metal grid at the front reflects some of the incident light. During radiation, additional reflection losses occur. Different indices of refraction cause additional reflection losses to occur as radiation moves from the air into the

semiconductor material. Antireflection layer applied to the surface reduces these losses.

- The solar radiation has a broad spectrum distribution, meaning that it comprises photons of various energy. Photons whose energies are below the bandgap are not absorbed and go to waste. Electron-hole couples won't form since the energies are insufficient to ionise electrons. Regardless of how much energy a photon has in excess of the band gap, only energy that is sufficient to fill the band gap is beneficial. The extra energy is released into the crystal lattice as heat.
- The photocurrent increases with decreasing bandgap because it is directly proportional to the amount of photons absorbed per unit of time. Yet, the bandgap also establishes the p-n junction's maximum diffusion voltage. A modest open-circuit voltage results from a narrow bandgap. Because the electrical power is determined by the sum of the current and voltage, very narrow bandgaps have low efficiency due to the low output power they produce. The open-circuit voltage will be high for big bandgaps. Just a little portion of the sun spectrum will be absorbed, though. As a result, the photocurrent only reaches modest levels in this situation. Once more, the result of current and voltage is negligible.
- The dark current  $I_0$  exceeds the value predicted by theory. As a result, the open-circuit voltage is decreased.
- Not all created charge carriers are collected; some of them merge. Charge carriers like to combine again near flaws, such as crystal lattice flaws or contaminants. In order to give the highest purity, source material must have a high crystallographic quality. The crystal structure is also severely perturbed near the semiconductor material's surface, where a zone of increased recombination is formed.
- The fill factor is always smaller than one (theoretical max. value about 0.85).
- Resistance in series and parallel causes the fill factor to decrease.

[1], [6], [2], [3], [4]

## 1.2. Modules History and Technology

A PV module consists of several interconnected solar cells encapsulated into a single, long-lasting, stable unit. The key purpose of encapsulating a set of electrically connected solar cells is to protect them and their interconnecting wires from typically harsh environment in which they are used. For example, solar cells, since they are relatively thin, are prone to mechanical damage unless protected. In addition, the metal grid on the top surface of the solar cell and the wires interconnecting the individual solar cells may be corroded by water or water vapor.

Many different types of PV modules exist, and the module structure is often different for different types of solar cells or for different applications. For example, amorphous silicon solar cells are often encapsulated into a flexible array, while bulk silicon solar cells for remote power applications are usually rigid with glass front surfaces. The most common modules have either 60 cells or 72 cells with three bypass diodes. 60 cell modules were originally designed for ease of handling in residential applications and heavier 72 cell modules for large utility installations where cranes and hydraulic lift are available. However, it is quite possible to use 72 cell modules in residential installations so long as the rest of the system is designed to handle the large size. Module lifetimes and warranties on bulk silicon PV modules are over 20 years, indicating the robustness of an encapsulated PV module. A typical warranty will guarantee that the module produces 90% of its rated output for the first 10 years and 80% of its rated output up to 25 years.

### 1.2.1. Photovoltaic Modules Composition

Most PV bulk silicon PV modules consist of a transparent top surface, an encapsulant, a rear layer and a frame around the outer edge. In most modules, the top surface is glass, the encapsulant is EVA (ethyl vinyl acetate) and the rear layer is Tedlar, as shown in Figure 13.

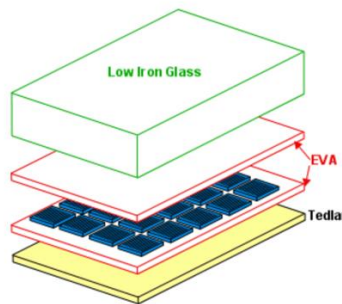


Figura 13: Typical Bulk Silicon Module Materials

The front surface of a PV module must have a high transmission in the wavelengths which can be used by the solar cells in the PV module. For silicon solar cells, the top surface must have high transmission of light in the wavelength range of 350 nm to 1200 nm. In addition, the reflection from the front surface should be low. While theoretically this reflection could be reduced by applying an anti-reflection coating to the top surface, in practice these coatings are not robust enough to withstand the conditions in which most PV systems are used. An alternative technique to reduce reflection is to "roughen" or texture the surface. However, in this case the dust and dirt are more likely to attach themselves to the top surface, and less likely to be dislodged by wind or rain. These modules are not therefore "self-cleaning", and the advantages of reduced

reflection are quickly outweighed by losses incurred due to increased top surface soiling. In addition to its reflection and transmission properties, the top surface material should be impervious to water, should have good impact resistance, should be stable under prolonged UV exposure and should have a low thermal resistivity. Water or water vapor ingress into a PV module will corrode the metal contacts and interconnects, and consequently will dramatically reduce the lifetime of the PV module. In most modules the front surface is used to provide the mechanical strength and rigidity, therefore either the top surface or the rear surface must be mechanically rigid to support the solar cells and the wiring. There are several choices for a top surface material including acrylic, polymers and glass. Tempered, low iron-content glass is most used as it is low cost, strong, stable, highly transparent, impervious to water and gases and has good self-cleaning properties.

An encapsulant is used to provide adhesion between the solar cells, the top surface, and the rear surface of the PV module. The encapsulant should be stable at elevated temperatures and high UV exposure. It should also be optically transparent and should have a low thermal resistance. EVA (ethyl vinyl acetate) is the most used encapsulant material. EVA comes in thin sheets which are inserted between the solar cells and the top surface and the rear surface. This sandwich is then heated to 150 °C to polymerize the EVA and bond the module together.

Regarding the rear surface the key characteristics of the PV module are that it must have low thermal resistance and that it must prevent the ingress of water or water vapor. In most modules, a thin polymer sheet, typically Tedlar, is used as the rear surface. Some PV modules, known as bifacial modules, are designed to accept light from either the front or the rear of the solar cell. In bifacial modules both the front and the rear must be optically transparent.

A final structural component of the module is the edging or framing of the module. A conventional PV module frame is typically made of aluminium. The frame structure should be free of projections which could result in the lodgement of water, dust or other matter.

It is with this premise, that this research may continue and move on to the cells' connection inside a PV module. In photovoltaic modules of any type, cells can be connected in series or parallel each other to form a single component.

Due to manufacturing differences, the cells are not the same, resulting in different current or voltage output. This gives rise to the so-called 'mismatching', which induces losses within the module itself. The mismatching of production between cells can also be caused by damage or shading of the cells. In the case of cell being shaded, it would no longer behave as a generator, with possible damage to the cell (hot-spot). In the case of partial shading of a cell, the current flowing through the module is equal to that which this cell would produce if taken individually, with a considerable reduction in

the power output of the module. To overcome these problems, diodes known as by-pass diodes are inserted between group of cells, with the function of protecting any non-operational cells and isolating the individual module in the event malfunction. The series connection of cells with the by-pass diode technology is shown in Figure 14.

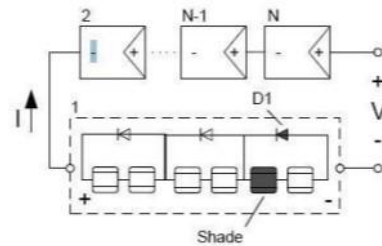


Figura 14: Darkned Cell and By-pass Diode

When several modules are connected in series, a string is formed in order to achieve the nominal voltage; several strings re connected in parallel to achieve the desired power output. In series with each string, a blocking diode is inserted to prevent unwanted current recirculation if the power output of the individual strings is not balanced. The connection of strings in parallel with bypass and blocking diodes is shown in Figure 15. [1] [2], [4]

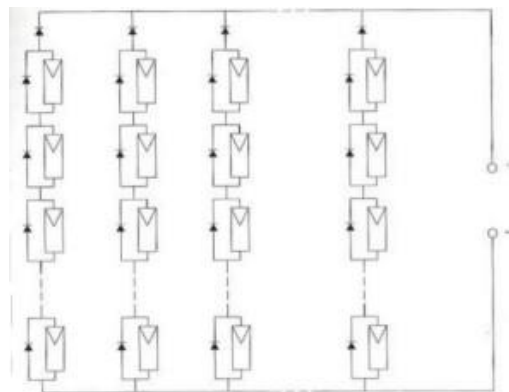


Figura 15: Connection of Strings in Parallel with Bypass and Blocking Diodes

### 1.2.2. Photovoltaic Module Characteristic Curves

The electrical behavior of the solar panels under homogeneous radiation of all PV cells is given by the current-voltage and power-voltage curves, shown in Figure 16. The I-V characteristic shows all the possible working points, it can be observed that the output power does not have a linear behavior and the maximum value of voltage and current are respectively  $V_{oc}$  and  $I_{sc}$ , nevertheless, at these points there is not power produced by the solar cell. The maximum value of the voltage is proportional to the

logarithm of the radiation level whereas the maximum value of the current is proportional to the radiation level.

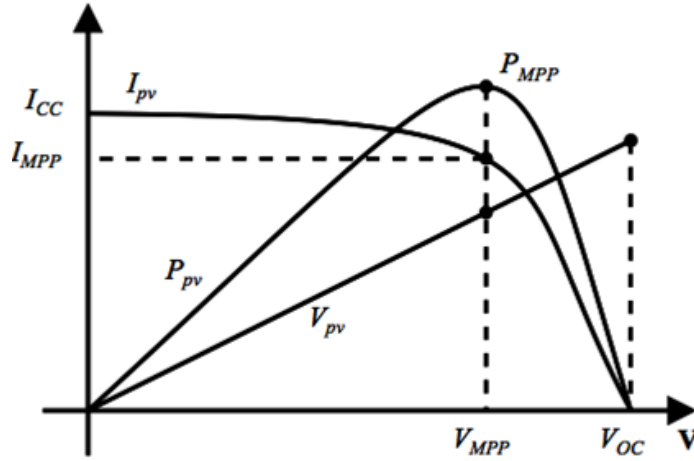


Figure 16: I-V and P-V Characteristics Curves of a Solar Cell

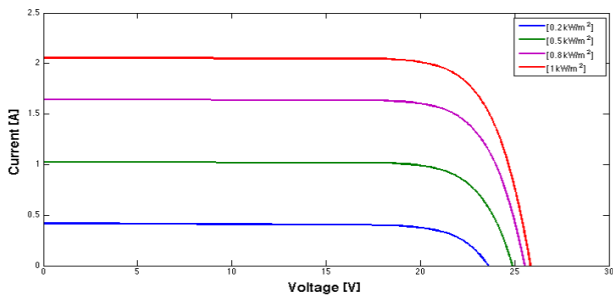
As explained previously, although the current has its maximum at the short-circuit point, the voltage is zero and thus the power is also zero. The situation for current and voltage is reversed at the open-circuit point, so again the power is zero. In between, there is one particular combination of current and voltage, for which the power reaches a maximum. The so-called maximum power point (MPP) represents the working point, at which the solar cell can deliver maximum power for a given radiation intensity. It is situated near the bend of the I-V characteristic curve. The corresponding values of  $V_{MPP}$  and  $I_{MPP}$  can be estimated from  $V_{oc}$  and  $I_{sc}$  by means of Equation 7 and Equation 8.

$$V_{MPP} = (0.75 - 0.9) V_{oc} \quad (7)$$

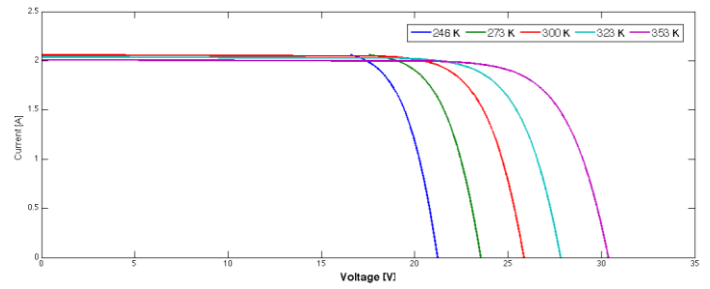
$$I_{MPP} = (0.85 - 0.95) I_{sc} \quad (8)$$

This analysis gives a hint on how the I-V characteristics is dependent on the solar irradiation level and the temperature. As it is observable from Figure 17 (a) and Figure 17 (b) the current is influenced by the irradiation level, whereas the voltage is influenced by the temperature.





(a)



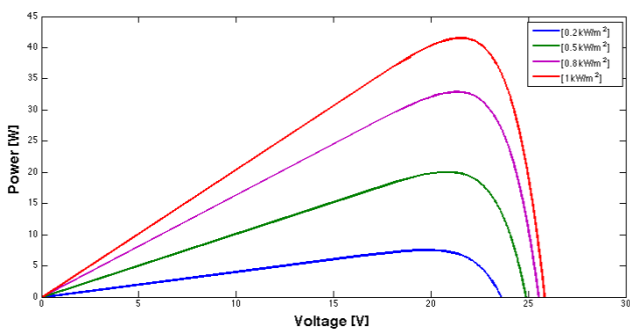
(b)

Figure 17: (a) I-V Curve dependence on the solar irradiation level, (b) I-V curve dependence on temperature

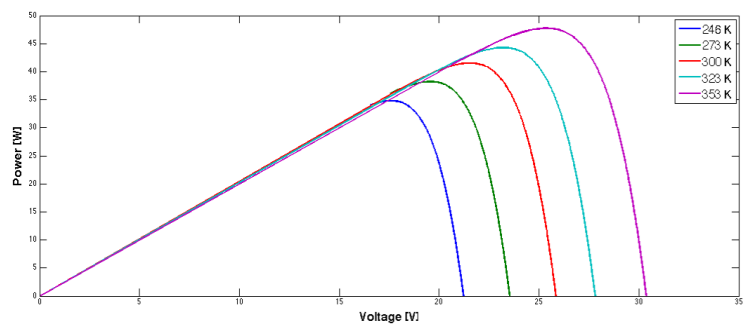
The power curve  $P-V$  is given by the product of the current and voltage in each point of the  $I-V$  curve. It can be noted in the Figure 16, that the power increase as the voltage  $V$  increases until is reached the value  $V_{MPP}$ , after this value the power starts to decay as the voltage value gets closer to the  $V_{oc}$ . The maximum power depends on the value of  $V_{oc}$  and  $I_{sc}$ , as previously explained, and this is confined in the filling factor. The  $FF$  is a parameter that describes the form of the  $I-V$  curve, in particular it describes how “square” this characteristic curve is. The filling factor is a key factor to evaluate the performance of a solar panel, as it was explained the previous chapter, and its value is typically 0.6-0.8.

Another striking parameter for describing the efficiency of the solar panel is the Efficiency of energy conversion  $\eta$ . It corresponds to the amount of energy that is actually converted into electric energy by the system.

As it was observed previously in this chapter, an increase in the temperature will have a decreasing effect on the output voltage, whereas a decrease in the solar radiation level will reduce the output current. Knowing that the power is the product of the voltage and current, the  $P-V$  current curve is also under the influence of these two factors, as shown in Figure 18 (a) and (b). [1], [3]



(a)



(b)

Figura 18: (a) P-V curve dependence on solar irradiation level, (b) P-V curve dependence on temperature

### 1.2.3. First Photovoltaic Modules Generation

In the most photovoltaic cells currently on the market, the active material is silicon. In monocrystalline silicon, each cell is made from homogenous, high-purity crystal. A monocrystalline solar panel is simply a solar panel made from monocrystalline solar cells or “wafers.” Monocrystalline wafers are made from a single silicon crystal that is formed into a cylindrical ingot. Although these panels are generally thought of as a premium solar product, the main advantages of monocrystalline panels are higher efficiencies and sleeker aesthetics. Since a monocrystalline cell is composed of a single crystal, the electrons that generate a flow of electricity have more room to move. As a result, monocrystalline solar cells are more efficient than their polycrystalline solar cell counterparts. An alternative to monocrystalline silicon is to make modules from polycrystalline silicon. Polycrystalline solar panels are also made from silicon. However, instead of using a single crystal of silicon, manufacturers melt many fragments of silicon together to form the wafers for the panel. Polycrystalline solar cells are also referred to as “multi-crystalline,” or many-crystal silicon. Polycrystalline solar panels generally have lower efficiencies than monocrystalline cell options because there are many more crystals in each cell meaning less freedom for the electrons to move. Due to the easier manufacturer process, these panels have a lower price point on average. In addition, polycrystalline solar panels tend to have a blue hue instead of the black hue of monocrystalline solar panels. [2], [4], [7]



Figura 19: Monocrystalline silicon panel (left) and polycrystalline silicon panel (right)

### 1.2.4. Second Photovoltaic Modules Generation

Thin-film solar panels use a 2nd generation technology varying from the crystalline silicon (c-Si) modules, which is the most popular technology. Thin-film solar cells (TFSC) are manufactured using a single or multiple layers of PV elements over a

surface comprised of a variety of glass, plastic, or metal. Thin-film solar panels require less semiconductor material in the manufacturing process than regular crystalline silicon modules, however, they operate fairly similar under the photovoltaic effect. This effect causes the electrons in the semiconductor of the thin-film PV module to move from their position, creating an electric flow, that can be harnessed into electricity through an external circuit. Thin-film solar panels are manufactured using materials that are strong light absorbers, suitable for solar power generation. The most commonly used ones for thin-film solar technology are cadmium telluride (CdTe), copper indium gallium selenide (CIGS), amorphous silicon (a-Si), and gallium arsenide (GaAs). The efficiency, weight, and other aspects may vary between materials, but the generation process is the same.

CdTe solar cells, which composition is shown in Figure 20, are manufactured using absorber layers comprising a p-n heterojunction, which combines a p-doped Cadmium Telluride layer and an n-doped CdS layer that can also be made with magnesium zinc oxide (MZO). To deposit materials on the substrate, manufacturers use the vapor-transport deposition or the close-spaced sublimation technique. On top of the absorber layer, CdTe thin-film solar cells include a Transparent Conductive Oxide (TCO) layer usually made with fluorine-doped tin oxide (SnO<sub>2</sub>:F) or a similar material. The electrical contact for these cells is made with zinc telluride (ZnTe), and the materials are placed over a metal or carbon-paste substrate. CdTe thin-film solar panels reached a 19% efficiency under Standard Testing Conditions (STC), but single solar cells have achieved efficiencies of 22.1%. This technology currently represents 5.1% of the market share worldwide, falling second only under crystalline silicon solar panels that hold 90.9% of the market. The cost for CdTe thin-film solar panels rounds the \$0.40/W.

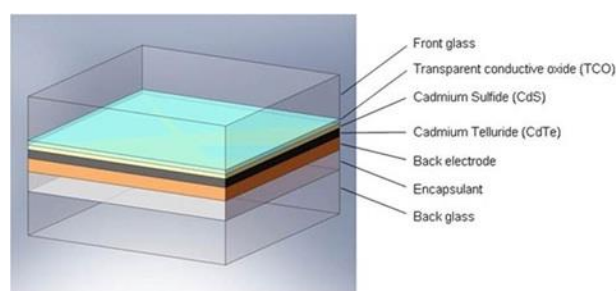


Figura 20: Composition of CdTe solar panel

CIGS thin-film solar cell, shown in Figure 21, are manufactured by placing a molybdenum (Mo) electrode layer over the substrate through a sputtering process. The substrate is usually manufactured with polyimide or a metal foil.

The absorbing layer is manufactured by combining a p-n heterojunction. The P-doped layer is made with copper indium gallium selenide (CIGS), placed above the electrode, and the CdS n-doped buffer is formed by chemical-bath deposition. To protect the

absorbing layer of the CIGS thin-film solar panel, a layer of Intrinsic Zinc Oxide (i-ZnO) is placed above the CdS buffer. The materials are finally covered with a thick AZO compound layer made with Aluminium doped Zinc Oxide (Al: ZnO), acting as the TCO layer to protect the cell.

The first CIGS thin-film solar panel manufactured by NREL reported a 17.1% efficiency, but the most efficient one ever created reported an efficiency of 23.4% and was made by Solar Frontier in 2019. The CIGS technology could be even more promising in the future since these materials can achieve a theoretical efficiency of 33%.

CIGS modules are not as popular for regular applications, being mostly used for space applications due to their resistance to low temperatures and great performance under low-intensity light conditions found in space. The cost is relatively more expensive than for other technologies, with a current price slightly above \$0.60/W, but future manufacturing generations promise to reduce the cost for these panels.

While CIGS thin-film solar panels have not become as popular as CdTe panels in the market, CIGS technology still holds 2.0% of the PV market share. Considering that thin-film solar modules only hold around 10% of the market, this is still quite popular as a thin-film solar technology.

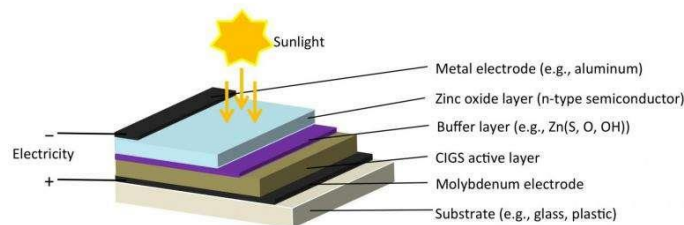


Figura 21: Composition of CIGS solar panel

Unlike other thin-film solar panels, amorphous silicon (a-Si) modules, which composition is shown in Figure 22, do not include an n-p heterojunction, but a p-i-n or n-i-p configuration, which differs from the n-p heterojunction by adding an i-type or intrinsic semiconductor. There are two routes to manufacture amorphous silicon (a-Si) thin-film solar panels, by processing glass plates or flexible substrates. Efficiency for a-Si solar cells is currently set at 14.0%.

Disregarding the route taken to manufacture amorphous silicon (a-Si) thin-film solar panels, the following steps are part of the process: first, the substrate is conditioned, the TCO and back reflector are placed under the deposition process, and then thin hydrogenated amorphous silicon (a-Si:H)-based layers are placed onto the electrodes, and the cells are connected in a monolithic series via laser scribing and silicon layers. The module is finally assembled and encapsulated, applying framing and electrical connections.

While manufacturing amorphous silicon (a-Si) requires an inexpensive material in low quantities, the price is relatively expensive, since the conductive glass for these panels is expensive and the process is slow, making the total cost of the panel to be set at \$0.69/W. This technology currently holds 2.0% of the retail market for PV modules.

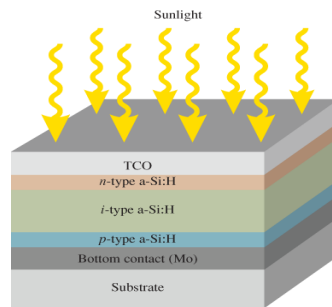


Figura 22: Composition of a-Si solar panel

Finally, the manufacturing process for GaAs thin-film solar cells is more complex than for regular thin-film solar cells and its composition is shown in Figure 23.

The first step is to grow the material. During this step, GaAs buffers are grown on Si substrates by being submitted to several temperature changes and different chemical processes, to finally create the layers for the cell. After the GaAs buffer grows, the substrate is processed for the fabrication of the cell. The first step is to deposit a Platinum (Pt)/Gold (Au) layer (10/50 nm) which will serve as the bonding material and electrode for the GaAs solar cell, and then a bonding process is performed on the substrate. After the bonding process is completed, the GaAs epitaxial layer that grew on the Si substrate is placed over the new substrate. To complete the assembly process a Pt/Titanium (Ti)/Pt/Au layer of 20/30/20/200 nm is deposited on the top contact layer through electron beam evaporation.

Since GaAs PV cells are multijunction III-V solar cells composed of graded buffers, they can achieve high efficiencies of up to 39.2%, but the manufacturing time, cost for the materials, and high growth materials, make it a less viable choice for terrestrial applications. The rated efficiency for GaAs thin-film solar cells is recorded at 29.1%.

The cost for these III-V thin-film solar cells rounds going from \$70/W to \$170/W. [2], [4], [8]

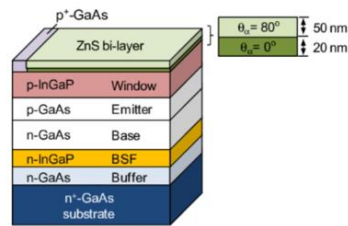


Figura 23: Composition of GaAs solar panel

### 1.2.5. Third Photovoltaic Modules Generation

Organic photovoltaic (OPV) solar cells, shown in Figure 24, aim to provide an Earth-abundant and low-energy-production photovoltaic (PV) solution. This technology also has the theoretical potential to provide electricity at a lower cost than first- and second-generation solar technologies. Because various absorbers can be used to create colored or transparent OPV devices, this technology is particularly appealing to the building-integrated PV market. Organic photovoltaics have achieved efficiencies near 11%, but efficiency limitations as well as long-term reliability remain significant barriers.

Unlike most inorganic solar cells, OPV cells use molecular or polymeric absorbers, which results in a localized exciton. The absorber is used in conjunction with an electron acceptor, such as a fullerene, which has molecular orbital energy states that facilitate electron transfer. Upon absorbing a photon, the resulting exciton migrates to the interface between the absorber material and the electron acceptor material. At the interface, the energetic mismatch of the molecular orbitals provides sufficient driving force to split the exciton and create free charge carriers (an electron and a hole).

The low efficiencies of OPV cells are related to their small exciton diffusion lengths and low carrier mobilities. These two characteristics ultimately result in the use of thin active layers that affect overall device performance. Furthermore, the operational lifetime of OPV modules remains significantly lower than for inorganic devices.

OPV cells are categorized into two classes: Small-molecule OPV cells and Polymer-based OPV cells.

Small-molecule OPV cells use molecules with broad absorption in the visible and near-infrared portion of the electromagnetic spectrum. Highly conjugated systems are typically used for the electron-donating system such as phthalocyanines, polyacenes, and squarenes. Perylene dyes and fullerenes are often used as the electron-accepting systems. These devices are most commonly generated via vacuum deposition to create bilayer and tandem architectures. Recently, solution-processed small-molecule systems have been developed.

Polymer-based OPV cells use long-chained molecular systems for the electron-donating material (e.g., P3HT, MDMO-PPV), along with derivatized fullerenes as the electron-accepting system (e.g., PC60BM, PC70BM). Like small-molecule OPV cells, these systems have small exciton diffusion lengths. However, this limitation is circumvented by a high interface surface area within the active device.

Dye-sensitized solar cells are a hybrid organic-inorganic technology that uses small-molecule absorber dyes. These dyes adsorb onto a suitable electron-accepting material, such as titanium dioxide or zinc oxide, along with an electrolyte to regenerate the dye. [2] [4] [9]

The main benefits promised by OPV solar cells include:

- Low-cost manufacturing: Soluble organic molecules enable roll-to-roll processing techniques and allow for low-cost manufacturing.
- Abundant materials: The wide abundance of building-block materials may reduce supply and price constraints.
- Flexible substrates: The ability to be applied to flexible substrates permits a wide variety of uses.

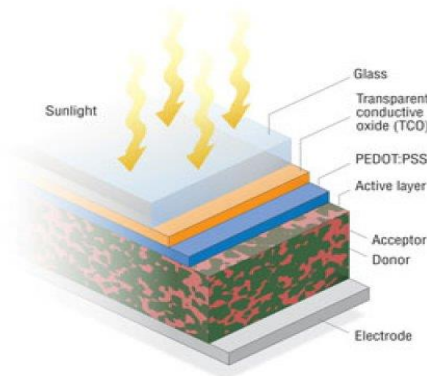


Figura 24: Composition of OPV solar panel

## 1.3. Inverters Technology and Configuration

### 1.3.1. Inverters General Characteristics

The conversion group from DC to AC (constituted by one or more inverters), working as a current generator, implements the conditioning and the control of the transferred power. The input voltage value and the input current values of the inverters must be

compatible with those of the photovoltaic plant to which they are connected. Whereas, the output voltage value and the output frequency value must be compatible with those of the distribution grid to which the inverters are connected.

The conversion group is based on forced-switching inverters (PWM technique) and it is able of fully automatic operation, following the maximum power point (MPPT) of the PV plant.

The most relevant data that permit the sizing of the PV plant and the choosing of the inverter are the following ones:

- Rated power and maximum power on DC side
- Rated current and maximum current on DC side
- Rated voltage and maximum voltage on DC side
- Rated power on AC side and maximum power that the conversion group can deliver continuatively; In addition, it is necessary to know the ambient temperature range at which such power can be delivered
- Distortion factor and power factor
- maximum current value on CA side
- Peak efficiency and input/output conditions at which maximum conversion efficiency is obtained
- Efficiency at part load (5,10,20,30,50%) and at 100% of the nominal power of the conversion unit, as well as for the so-called "European efficiency"

The European efficiency coefficients is given by the weighted average of the efficiencies measured at different power values: 5%, 10%, 20%, 30%, 50%, 100% of the maximum power. It is defined by means of Equation (9).

$$\eta_{euro} = 0.03 \cdot \eta_{5\%} + 0.06 \cdot \eta_{10\%} + 0.13 \cdot \eta_{20\%} + 0.10 \cdot \eta_{30\%} + 0.48 \cdot \eta_{50\%} + 0.20 \cdot \eta_{100\%} \quad (9)$$

For clarity, the efficiency graph of a 3kW inverter and its European efficiency coefficient is shown in Figure 25.



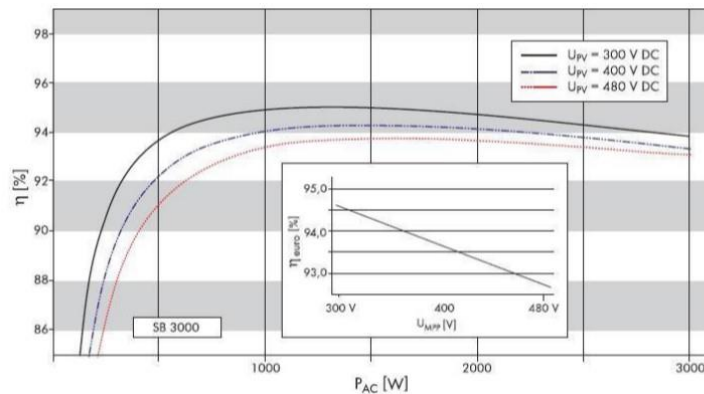


Figura 25: Efficiency of a 3kW inverter and European efficiency

The inverter must be designed to prevent, as well as in electrical panels, condensation from forming in the IP65 enclosure; this is usually ensured by proper design of the distances between electronic boards.

It is also important to pay attention to the interferences between inverters. Inverters for photovoltaic applications are made with semiconductor devices that switch at high frequency; during these switchings, fast voltage transients will be generated that can propagate to nearby electrical circuits and equipment, resulting in interference. Interference can be conducted or radiated. Inverters must have CE marking; this means that it is presumable that they respect the border limits of the interference values. Furthermore, the laboratory verifications are made in standard condition and are not necessarily repeated at the installation site, where there could be sensitive instruments. Therefore, to minimize the interferences, it should be taken into account the earth conductor and the position of the inverter, that should be as far upstream as possible with respect to the PV plant, considering separate cable ducts.

If the photovoltaic system is connected to the low voltage grid, inverters must have a metallic separation between the AC side and the DC side to avoid direct current injection into the grid. Otherwise, if the PV plant has a nominal power lower than 20kW, it is possible to install a particular protection, instead of the metallic barrier, which acts when the value of the overall continuous component exceeds the rms value of the overall fundamental component of the converters by 0.5 percent.

Once the type of grid connection is identified (MV or LV, single-phase or three-phase), the input and output voltage and frequency ratings need to be evaluated. The input voltage must be chosen taken into consideration the voltage of the photovoltaic strings. For the output voltage, it is necessary to take into account that the voltage and frequency values must be within the operating range indicated on the nameplate of the inverter; For national distribution networks these are usually 230V 50Hz (400V in three-phase).

Regarding the input voltage, it should be taken into account that whether the PV array is configured by adapting it to the preferred inverter model or whether the inverter suitable for the adopted string configuration is to be chosen, the extreme operating conditions should be carefully evaluated in order to have a proper operation of the inverter.

The maximum applicable DC input voltage is defined for each inverter model. The no-load voltage of the PV array, estimated at the minimum expected operating temperature, must, therefore, be less than this voltage value. On some inverter models, the input stage consists of a capacitor bank, so insertion on the PV array causes a short current inrush, equal to the short-circuit current of the PV array connected to the terminals, which should not trip any internal protections.

Each model of inverter is characterized by a range of input voltage values of normal operation; it is important, for the purpose of having the highest possible efficiency, that the conversion unit manages to operate the photovoltaic field always in the conditions of maximum power. therefore, the minimum value of operation is the most important value, as it indicates the minimum DC input voltage that keeps the control logic on and allows the correct supply in the distributor's network even at low values of solar irradiation.

When the temperature of the PV cell arises, the maximum power voltage of the PV plant decrease. Therefore, when the inverter is chosen, it is necessary to check if the PV plant voltage at the maximum possible temperature is higher than the minimum voltage at which the inverter works in the maximum power point.

Some inverters adopt a minimum operating value for the input DC-side voltage, which varies dynamically with the amplitude of the distributor grid voltage: as the distributor grid voltage increases, the lower operating limit is raised. In this case, the distributor grid voltage normally present at the point of delivery and its effect on the inverter's DC operation must be evaluated to prevent a sizing performed on nominal values alone from causing the inverter to fail to operate in the maximum power condition.

In order to investigate the energy output of the conversion unit, typical inverter efficiency curves, normalized with respect to the rated output power, are presented in Figure 26.

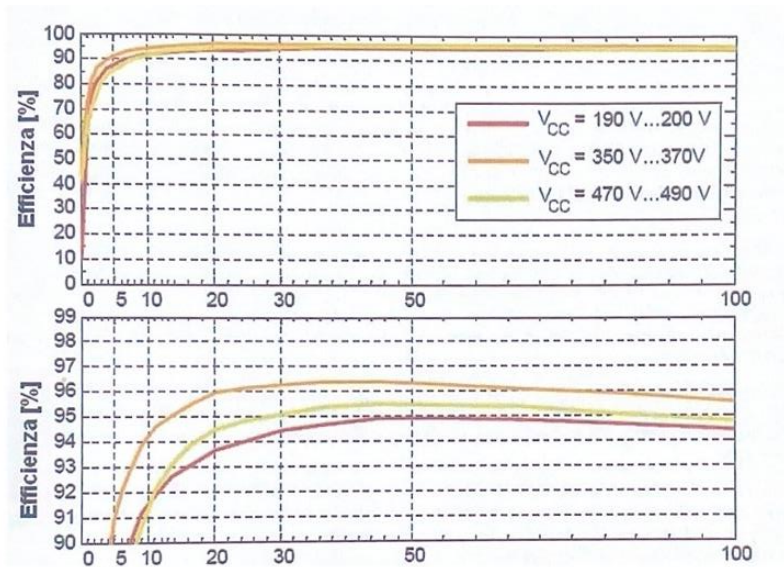


Figura 26: Typical inverter efficiency (0%-100%) and details between 90% and 100%

It is evident from the figure that the maximum output is obtained between 40% and 80% of the inverter nominal power, that corresponds to the power level at which the inverter works the most of its lifetime. The maximum output value is indicated as  $\eta_{max}$  in the user guide provided by the manufacturer.

It should be noted that the inverter maximum output value is not a sufficient parameter for sizing purposes because it does not consider that the inverter is working at partial load, as is the case in most cases. In light of this, it can be considered the European efficiency coefficient, analyzed previously in the chapter.

To conclude, another coefficient useful for the check of the invert quality is the guaranteed minimum performance value, that is given by the ratio between the output power of the AC-side and the input power on the DC-side, considering  $P_{ca} > 30\%$  of the nominal output power. [6], [3], [10]

### 1.3.2. Conversion Unit Configurations

When choosing the type of conversion unit, it should be taken into account that the type of connection to the distributor's grid depends on the power of the system (IEC 11-20; V1):

- for rated power of the conversion unit  $> 6\text{kW}$ , the three-phase connection to the grid is adopted
- for power ratings  $< 6\text{kW}$ , the single-phase connection can be adopted

If the three-phase connection, used in Verdeto's design which will be discussed in the following chapters, is adopted, this can be achieved by using inverters with three-phase output or single-phase inverters in a three-phase configuration (typically connected between a grid phase and the neutral).

Depending on the configuration of the PV system, the most appropriate components for local conditions should be chosen at the sizing stage. The choice of the type of inverter assumes importance at this stage: in particular, it should be decided whether to spread the power of the PV generator over several inverters (multi-inverter conversion group) or to use a single inverter (centralized inverter conversion group). Each solution has advantages and disadvantages. In the specific case of Verdeto, the chosen configuration is a multi-inverter conversion group, as will be analyzed in the following chapters.

Typically, high-power inverters have lower costs per unit of power than lower-power inverters, due to the fact that it is easier to achieve high efficiencies with high-power machines. In contrast, smaller size inverters are generally suitable for outdoor installations, as in the case of Verdeto. They also allow the simplification of DC wiring by eliminating the need for string parallel panels near PV modules.

To conclude, in terms of the reliability of the entire generating plant, while the probability of failure in multi-inverter conversion systems might be higher being the greater number of components present, the downtime of a centralized inverter causes the total loss of plant production.

The choice of the inverter model and size must be done considering the nominal power of the PV plant at which it is connected. It is possible to estimate the inverter size, choosing between 0,8 and 0,9 of the ratio between the active power injected into the grid and the nominal power of the PV generator; This relationship considers the modules power decreasing in the real working conditions (working temperature, modules dirt, voltage drops on electrical connections, etc..) and the performance of the inverters. This ratio is highly influenced by the installation conditions of the modules that may vary the power generated. In light of this, the inverter is equipped with an automatic power output limitation, which makes it possible to limit the situation where the power output is higher than required.

Once the choice of the inverter is made, it should be considered the installation site. The inverter can be situated both indoor and outdoor, depending on the degree of protection. It is good practice that inverters installed outdoors should not be exposed to direct sunlight, this is to avoid unnecessary heating produced by incident solar energy.

After providing the inverter with a suitable environment for its degree of protection, adequate temperatures and ventilation must be ensured, as these alone are crucial to the inverter performance. Each inverter is characterized by an ambient temperature range within which it can safely operate and a reference temperature at which the power rating is defined. The reference temperature may not coincide with the operating temperature range. Moving away from the reference temperature, the inverter may limit the power output in order to keep the semiconductor temperature under control and safeguard its integrity. Excessive heating can lead to inverter shutdown due to overheating. Therefore, a careful assessment of the ambient temperature that will be established in the vicinity of the inverter is needed to understand whether at the times of highest output, which coincide with the hottest times of the day, the inverter will be able to feed the maximum available power into the grid. From the technical documentation provided by the manufacturer, the maximum temperature at which the power extracted from the PV array can be delivered can be derived, and if this is lower than the expected temperature, it is necessary to install the inverter in a different site.

Even if in this paper the conversion group is installed outdoor, it is useful to analyze the thermal dissipation of an inverter inside an electrical panel.

The thermal dissipation  $P_d$  of an inverter in an electrical panel is computed as Equation (10).

$$P_d = P_{nom} \cdot \frac{(1 - \eta_{100})}{\eta_{100}} \quad (10)$$

The dissipated power, that considers the inverter efficiency at the nominal power, must be added to the other dissipations to calculate the power that the electrical panel has to dissipate towards the outside. Each electrical box has a thermal resistance inversely proportional to its external surface area; therefore, the thermal jump from ambient to external is given by the following formula:  $\Delta T = R_{th} \cdot P_d$  and therefore, the final temperature of the electrical box is:  $T_{box} = T_{external} + \Delta T$ .

If the box temperature exceeds the maximum working temperature of the inverter, it is necessary to decrease the thermal jump by means of fans. To conclude, it is possible to calculate the flow rate of the fans using Equation (11). [6], [3], [10]

$$Q = 3,5 \cdot \frac{P_d}{\Delta T} \quad (11)$$

## 1.4. Solar Cables Characteristics

Electric cables used for photovoltaic systems must fulfil the following main requirements:

- have a nominal voltage compatible with the maximum voltage of the electrical system in which they are inserted
- have a conductor voltage that allows a current density and voltage drop below the limits prescribed by the applicable standards and predetermined at the design stage

The nominal voltage of a cable is the reference voltage for which the cable is designed and serves to define the electrical tests to which it must be subjected. The rated voltage is the combination of two values,  $U_0/U$ , expressed in volts:

- $U_0$  is the r.m.s. value between each insulated conductor and earth (metal covering of the conductor or surroundings)
- $U$  is the r.m.s. value between two phase conductors of a multi-core cable or single-core cable system.

The maximum voltage of a cable ( $U_m$ ) is the maximum concatenated voltage of a system (expressed in rms value) and is the highest value of voltage that can occur at any time and at any point of the system under regular operating conditions, not taking into account temporary voltage variations such as those due to faults or abrupt disconnections of important loads (IEC 20-13). [11], [12]

### 1.4.1. AC Cables Analysis

According to IEC Guide 20-67, Art. 2.3.1., in AC circuits the nominal voltage of the system must not exceed the nominal voltage of the cables. This condition applies to both the  $U_0$  value and the  $U$  value of the cable.

In practice, Equation (12) must be satisfied. [11] [12]

$$U_0/U \text{ of the cable} \geq U_0/U \text{ of the system} \quad (12)$$

### 1.4.2. DC Cables Analysis

According to IEC Guide 20.67 Art. 2.3.1., in DC circuits, the nominal system voltage must not exceed 1.5 times the nominal cable voltage. This condition applies to both the  $U_0$  value and the  $U$  value of the cable, which refer to rms values of the AC voltage. In other words, these standards indicate that, in DC circuits, the reference cable voltages are obtained from the  $U_0/U$  values multiplied by 1.5.

Cables according to CEI 20-91, on the other hand, can be used up to a maximum DC voltage of 1800V even to earth.

The maximum voltage of the electrical system, consisting of the DC circuits of a photovoltaic system, is given by the value of the no-load voltage of the PV generator at the minimum working temperature of the modules and is indicated by the value  $V_{oc,max}$ . It should be remembered that  $V_{oc,max}$  is the sum of the no-load voltages ( $V_{oc}$ ) of the photovoltaic modules connected in series (strings) at the minimum ambient temperature considered in the design.

The value of  $V_{oc,max}$  can be determined by means of the algorithm reported in the standard CEI EN 61829, which, however, presents application difficulties as it is necessary to know some characteristic parameters of the modules that are not always present in the datasheets.

For this reason, Equation (13) is difficult to verify due to the difficulty in determining the value of  $V_{oc,max}$ .

$$\text{Rated AC voltage of cables} \cdot 1,5 \geq V_{oc,max} \quad (13)$$

A simplified method to check whether the nominal voltage of DC cables is suitable for the maximum voltage of the photovoltaic electrical system, without performing a  $V_{oc,max}$  calculation, is given in TS 62257-7-1. In that document, taking into account that  $V_{oc,max}$  is always higher than the open circuit voltage of the PV generator at STC ( $V_{oc,array}$ ) and that this can be calculated as the product of the open circuit voltage at STC of the module (obtainable from the datasheet) times the number of modules constituting the individual string, it is stated that the nominal cable voltage must be 1.2 times  $V_{oc,array}$ . Therefore, Equation (14) has to be respected.

$$\text{Rated AC voltage of cables} \cdot 1,5 \geq 1,2 \cdot V_{oc,array} \quad (14)$$

Because of the above, since in photovoltaic generators the nominal cable voltage is  $U_0 = U$ , Equation (15) must be verified.

$$U_0 \cdot 1,5 \geq 1,2 \cdot V_{oc,array} \quad (15)$$

For example, cables with a rated voltage of 0.6/1kV are electrically suitable for use in DC circuits of a PV generator if it is verified that:

- accurate method according to EN 61829:

$$U_0 \cdot 1,5 \geq V_{oc,max}$$

$$600 \cdot 1,5 = 900\text{V in DC} \geq V_{oc,max}$$

- simplified method according to TS 62257-7-1:

$$U_0 \cdot 1,5 \geq 1,2 \cdot V_{oc,array}$$

$$600 \cdot 1,5 = 900\text{V in DC} \geq 1,2 \cdot V_{oc,array}$$

$$750\text{V in DC} \geq V_{oc,array}$$

It is advisable for the designer to calculate  $V_{oc,max}$  by the accurate method whenever possible.

In PV systems, DC cables are used to make connections between PV modules, string parallel boxes if present, and inverters (Figure 27).



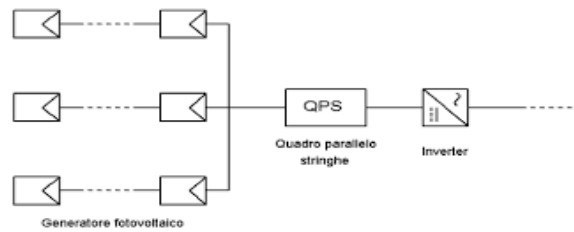


Figura 27: Links between modules, parallel switchboard and inverter

For the connection between the modules and the string parallel boxes, cables for photovoltaic applications are recommended according to IEC 20-91. The same type of cable may also be used, according to the assessment of the designer, for the connection between the parallel string switchboard and the inverter.

The standard CEI 20-91 defines the characteristics of electrical cables, with designation FG21M21, that can be used in DC connections between photovoltaic modules, parallel string switchboards and inverters.

FG21M21 cables have the following characteristics:

- conductor: tinned copper/aluminium wires
- insulation: halogen-free cross-linked elastometric compound type G21
- sheath: M21 type halogen-free cross-linked elastometric compound
- ambient temperature: -40 to 90 °C
- maximum overload temperature: 120 °C
- maximum short-circuit temperature: 250 °C
- maximum voltage  $U_m$ : 1.8kV DC also to earth
- estimated period of use: 25 years

The cables used in the DC section of a photovoltaic system must also have the following characteristics:

- maximum voltage compatible with the system voltage
- sufficient cross-section to limit voltage drops, in the section between the modules and the inverters, to within 2%.
- suitable for fixed outdoor and indoor installation, protected with external sheathing or within visible or recessed insulation pipes
- suitable for installation directly underground or in buried pipes in accordance with CEI 11-17
- resistant to water, UV, ozone, frost, chemicals and long service life

- high mechanical resistance
- ability to operate at the temperature achievable by the specific application

Cable dimensioning is carried out with two main goals in mind: to keep the voltage drop at the maximum operating current within the design limits and to ensure a satisfactory service life of the conductors and insulations subjected to the thermal effects caused by the passage of current for extended periods and under normal operating conditions. [11], [12]

## 1.5. Interface to MT Distribution Network

In this chapter, the last elements that make up a self-consuming, grid-connected photovoltaic system will be analyzed: the interface devices. In particular, the devices that allow interfacing and protection to the MV grid will be explained, since the Verdeto plant that will be analyzed in detail later is connected to the MV grid.

Photovoltaic systems connected to the distributor's grid always include the following components and subsystems:

- photovoltaic generator, consisting of the electrically connected modules with direct current output
- inverter, which converts the direct current into alternating current with a voltage and frequency compatible with those characteristic of the electricity grid
- interface system to the distributor's grid, consisting of the device and interface protection system, interposed between the DC/AC converter and the distributor's grid in order to safeguard the quality of the electrical service and avoid dangers to persons working on the grid and damage to equipment.

In Italy, the main regulatory reference for the connection of power generation systems to the MV electricity grid is the CEI 0-16 standard.

According to CEI 0-16, the maximum power of a photovoltaic system that can be connected to the electricity grid depends on the number of phases and the voltage of the grid, as well as the characteristics of the grid itself and the loads in it (Table 2).

Tabella 2: PV system power value that can be connected to the grid

Potenza [kW]	Livelli di tensione della rete del Distributore	Riferimenti
≤ 6	BT (in monofase)	CEI 11-20
≤ 100	BT	AEEG ARG/eit 99/08 CEI 0-16 (Tab. 4)
100 - 200	BT o MT (*)	CEI 0-16 (Tab. 4)
200 – 3 000	MT	CEI 0-16 (Tab. 4)
3 000 – 10 000	MT o AT (*)	CEI 0-16 (Tab. 4)
> 10 000	AT	CEI 0-16 (Tab. 4)

(\*) da concordare con il Distributore in funzione delle caratteristiche della rete e dei carichi in essa presenti

The general connection diagram of a production plant operating in parallel with the Distributor's grid with its interface/protection devices in accordance with CEI 0-16 is shown in Figure 28. [11]

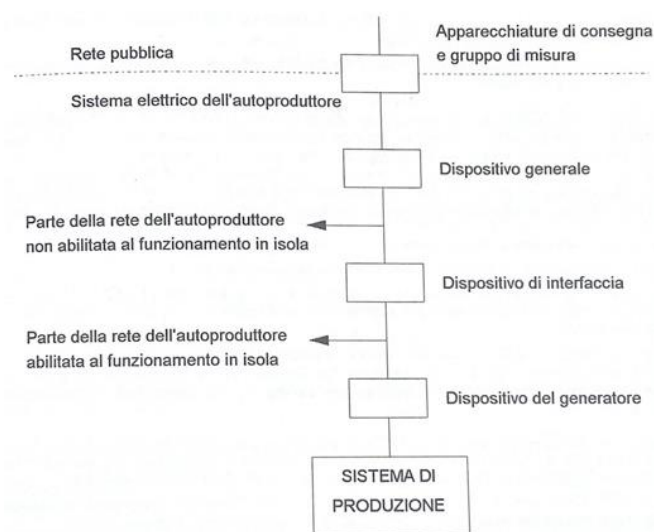


Figura 28: Scheme of general PV plant connected to the grid according to CEI 0-16

Considering Figure 28 the general characteristics of the three devices for the MT grid connection will be described in the next chapters.

### 1.5.1. General Devices Characteristics (DG)

The DG consists of a switching and disconnection device (installed at the origin of the user's network) whose opening, controlled by the general protection system, ensures the separation of the entire user's installation from the network. The DG intervenes in the event of a fault in the user's installation.

According to CEI 0-16 paragraph 8.5.11, the general device may consist of one of the following components acting on all phases and the neutral:

- three-pole switch in withdrawable execution with opening trip release
- three-pole switch with opening trip and three-pole disconnecter to be installed upstream of the switch

[11], [12]

### 1.5.2. Interface Protection Devices Characteristics (DDI)

The DDI consists of one or more switching devices (installed at the point of connection of the off-grid user's grid to the remaining part of the user's grid) the opening of which, controlled by the interface protection system, ensures the separation of the production plant from the grid, allowing the production plant itself to operate in self-consumption/islanding on the privileged loads.

The DDI intervenes in the event of a fault on the Distributor's grid.

The DDI must be 'intrinsically safe', i.e. it must be equipped with an opening coil in the event of a power failure. In the case of a three-phase system, the DDI, if it is unique, must be of the omni polar type.

The interface device, depending on the voltage level on which it is installed, may be constituted in the following manner, as indicated in CEI 0-16 paragraph 8.7.4.1:

- a three-pole circuit breaker in withdrawable execution with opening disconnection on power failure, or
- a three-pole circuit-breaker with a residual current device and a disconnecter installed upstream or downstream of the circuit-breaker

For systems with several generators, the DDI must normally be single and such that all generators are simultaneously excluded.

According to CEI 0-16 (Article 8.7.5.1), in photovoltaic installations, the Interface Protection System (SPI) associated with the DDI must comply with Annex E of the same CEI 0-16 standard and, must have the following characteristics:

- provides for frequency, voltage relays that guarantee the following protection and related regulations:
  - maximum voltage: value  $1.2 V_n$ ; fault extinction time  $\leq 170\text{ms}$  (which is typically achieved by an intentional delay of 100ms)
  - minimum voltage: value  $0.7 V_n$ ; fault extinguishing time  $\leq 370\text{ms}$  (typically achieved by means of an intentional delay of 300ms)
  - maximum frequency: value 50.3Hz; fault extinction time  $\leq 170\text{ms}$  (typically achieved by an intentional delay of 100ms)
  - minimum frequency: value 49.7Hz; fault extinction time  $\leq 170\text{ms}$  (typically achieved by an intentional delay of 100ms)
- the maximum/minimum frequency and maximum/minimum voltage protections must have as input proportional values of at least two MV concatenated voltages that can therefore be taken from the secondary of VTs connected between two MV phases or from LV concatenated voltages
- adjustments must take into account the voltage level at which the quantities are measured
- If several relays are used, the tripping of any one relay must cause the DDI to open.
- the regulation of the protections is the responsibility of the user on the basis of the regulating plan prepared by the distributor

[11], [12]

### 1.5.3. Generator Devices Characteristics (DDG)

Generator device: the DDG consists of a maneuvering device (installed at the output terminals of each generator of the production system) whose opening, controlled by a special protection system, determines the separation of the generating unit from the grid. The DDG is triggered by an internal generator fault.

According to CEI 0-16 paragraph 8.7.4.2, the generator device (DDG) can consist of one of the following components:

- a three-pole switch in withdrawable design with opening release, or
- a three-pole switch with opening trip and a disconnecter installed on the mains side of the switch

the DDG can perform the functions of the DDI, if it has the characteristics: as specified above. However, it is always necessary to have two circuit breakers in series with each other or, alternatively, a circuit breaker and a contactor between the generation and the distribution network. [11] [12]

## 2 Case of Study

### 2.1. Introduction: Self-consumption Photovoltaic Power Plant

Self-consumption can be described as the local use of PV electricity in order to reduce the supply of electricity from other producers. In practice, self-consumption ratio can vary from a few percent to a theoretical maximum of 100%, depending on the PV size and the local load profile. Given the diversity of policies allowing for self-consumption that are being implemented worldwide, in order to classify all self-consumption schemes, several parameters have been chosen, covering all aspects of self-consuming PV electricity. These parameters aim at categorizing all kinds of policies supporting self-consumption and to clarify the wording used in several countries, especially net-metering and net-billing schemes. Table 3 provides detailed information about parameters. Later in the chapter, the Italian regulations will be analysed in detail.

Tabella 3: Main self-consumption parameters

<b>PV Self-consumption</b>	<b>1</b>	Right to self-consume
	<b>2</b>	Revenues from self-consumed PV
	<b>3</b>	Charges to finance T&D
<b>Excess PV electricity</b>	<b>4</b>	Revenues from excess electricity
	<b>5</b>	Maximum timeframe for compensation
	<b>6</b>	Geographical compensation
<b>Other system characteristics</b>	<b>7</b>	Regulatory scheme duration
	<b>8</b>	Third party ownership accepted
	<b>9</b>	Grid codes and additional taxes/fees
	<b>10</b>	Other enablers of self-consumption
	<b>11</b>	PV System Size Limitations
	<b>12</b>	Electricity System Limitations
	<b>13</b>	Additional features

- **Right to self-consume:** this parameter identifies whether the electricity consumer has the legal right to connect a PV system to the grid and self-consume a part of its PV-generated electricity.
- **Revenues from self-consumed PV electricity:** this parameter is based on the source of revenue from each kWh of self-consumed PV electricity. It comprises not only the savings on the electricity bill but also possible additional revenues such as a self-consumption bonus/premium or green certificates.

- Charges to finance grid (distribution and transmission) costs: this parameter indicates whether the PV system owner must pay part of the total grid costs on the self-consumed electricity.
- Value of excess electricity: this parameter explains which compensation the PV system owner will receive when PV electricity is injected into the grid.
- Maximum timeframe for credit compensation: this parameter refers to schemes that allow credits for all electricity injected. Such credits can in general be used during certain period during which compensation is permitted.
- Geographical compensation: this parameter indicates whether consumption and generation can be compensated in different locations (e.g. “virtual net-metering”, “meter aggregation”, and “peer to peer”).

Let’s analyze in detail the Italian situation. In Italy self-consumption is allowed for all PV system sizes. For systems below 200kW (and even 500kW for plants installed starting from 2015), Italy has switched in 2009 from a net-metering mechanism to the so-called “Scambio sul posto(SSP)”. The SSP can be seen as a hybrid solution between a self-consumption system (real-time self-consumption) with some net-billing features (for the calculation of the “energy quota” and the “service quota”). After the end of the FiT law, net billing is the only scheme left. Above the 500kW limit, a pure self-consumption scheme is used.

With the SSP, the electricity fed into the grid is remunerated through an “energy quota” that is based on electricity market prices and a “service quota” that depends on the cost of grid services (transport, distribution, metering and other extra charges). Without SSP, the market prices apply for the electricity injected into the grid. Grid costs linked to self-consumed electricity are compensated for all plants under SSP scheme; for system bigger than 20kW, a fee is added to the bill to compensate partially the saved grid costs. The summary of the Italian parameters is shown in table 4.

Tabella 4: Italy’s self-consumption scheme

			Italy
PV Self-consumption	1	Right to self-consume	Yes
	2	Revenues from self-consumed PV	Savings on the electricity bill
	3	Charges to finance T&D	Yes, above 20 kW
Excess PV electricity	4	Revenues from excess electricity	SSP, net-billing based on energy and services; market price for selling
	5	Maximum timeframe for compensation	Self consumption, real time; SSP, advance payment twice per year
	6	Geographical compensation	On site (meter aggregation is allowed for some specific SSP cases)
Other System characteristics	7	Regulatory scheme duration	Unlimited
	8	Third party ownership accepted	Yes, with conditions for SSP
	9	Grid codes and additional taxes/fees	None
	10	Other enablers of self-consumption	None
	11	PV System Size Limitations	Self-consumption, none (below 20 MW for SEU); SSP, up to 500 kW
	12	Electricity System Limitations	None
	13	Additional features	None



## 2.2. Photovoltaic power plant: Project Verdeto 127.68kWp

This project deals with the design and construction of an electric power generation plant by photovoltaic conversion, with a rated capacity of 127.68 kW and a peak capacity of 127.68 kWp.

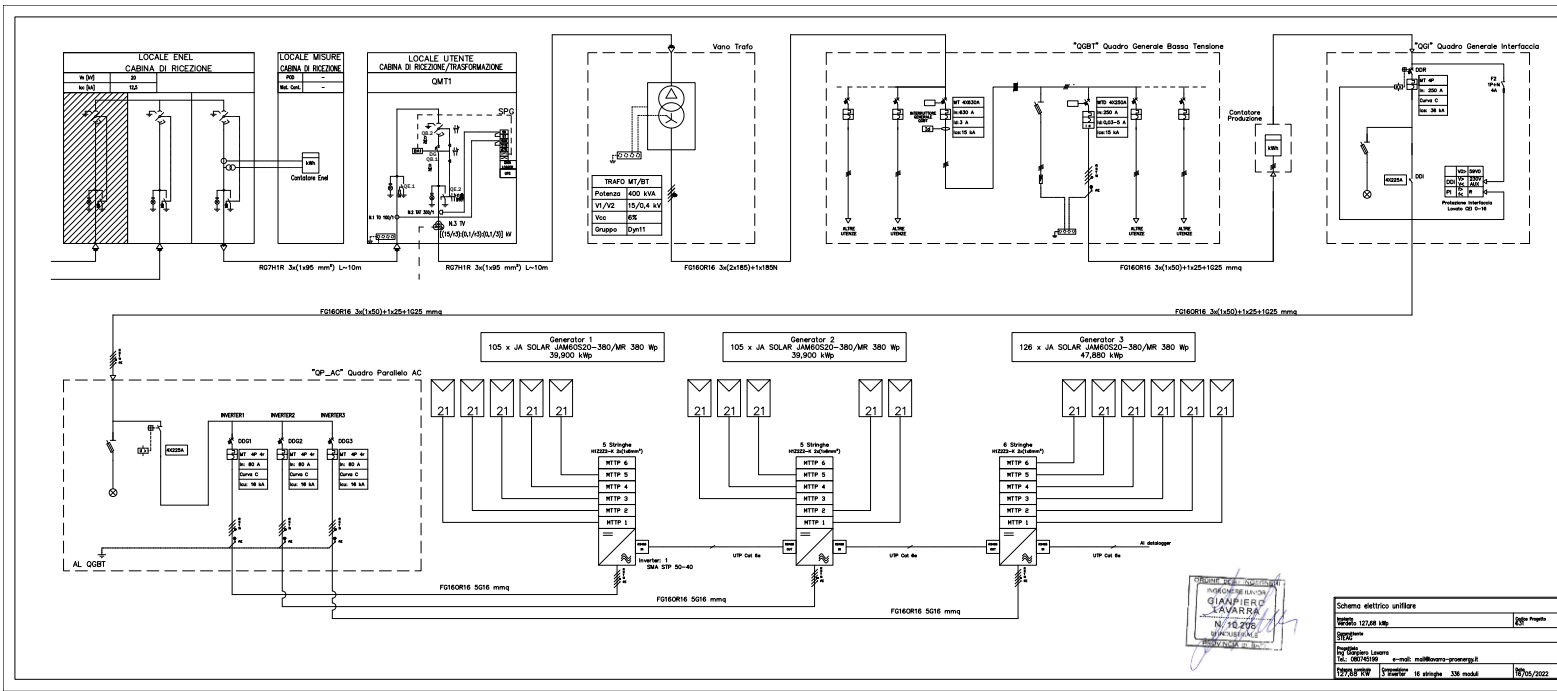


Figura 29: Single-line diagram of the photovoltaic power plant

Figure 29 shows the single-line diagram of the Verdeto photovoltaic generation plant. The three inverters to which the 16 strings of 21 modules each are connected are observed. The purpose of the following chapters will be the detailed analysis and sizing of the modules, inverters and cables. The sizing of the string parallel switchgear and the interface protection switchgear will not be the subject of the study, as this is the task of the subcontracted company and not the work done at STEAG Sens Italia.

### 2.2.1. Feasibility Analysis

#### 2.2.1.1. Location Analysis

The Verdeto photovoltaic plant rises on the roof of a building located in the Province of Piacenza 29010 Strada Verdeto, at a latitude of 044°57'07 "N and a longitude of 009°29'18 "E. Compared to sea level, the plant will have an elevation of 241m and will have an Albedo coefficient (reflection coefficient) of 0,2.

Figure 30 is a top-down photograph of the building on which the plant will stand (the ones with grey cover), you can see that there are no surrounding buildings that may shade the plant, since the built is the building having the greatest height.



Figura 30: Top-down photo of the building

In Figure 31 is shown a plan of the roof of the built-up area. It can be seen that the building is very simple and lends itself to the installation of a rooftop PV system.

It has a rectangular shape, the long side measures 56.20m while the short side measures 17.67m and has a height of 6.50m, for a total area of 993.054  $m^2$ .

The roof of the building is a sheet metal supported by 22 stringers that allow the stability of the plant.

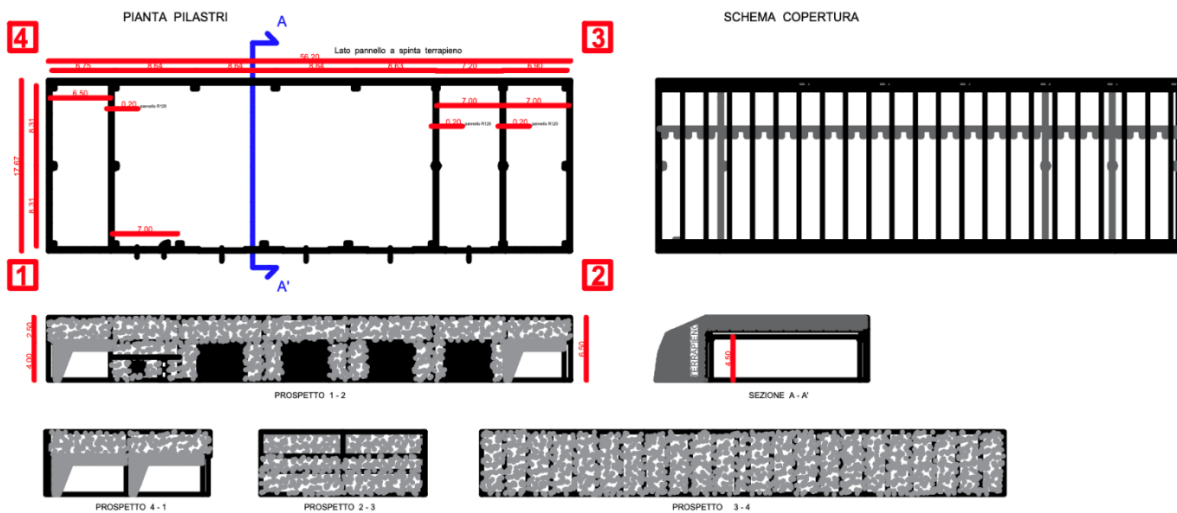


Figura 31: Roof cover extrapolated from Autocad

From this prior analysis, some features that favor the installation of a rooftop photovoltaic system can already be inferred:

- There is no risk of shading since the building is insulated
- Stable flat roof made of sheet metal, ideal for fixing substructures

As can be seen from Figure 32, the building is located near a medium-voltage connection box to the national grid, the connection is easy because of the lack of architectural barriers (rivers, height differences, streets, etc.).



Figura 32: Cabinet connection identification

### 2.2.1.2. Irradiation Analysis

The assessment of the available solar resource was based on the ENEA Standard, taking as a reference the location that has the historical solar radiation data in the immediate vicinity of Piacenza Province.

First, it is interesting to look at the graph in Figure 33, which represents the solar Cartesian diagram. As can be seen, the months in which the sun has a greater height are June, July and May. Also, as was to be expected, the hour when the sun occupies the highest position is noon of each month.

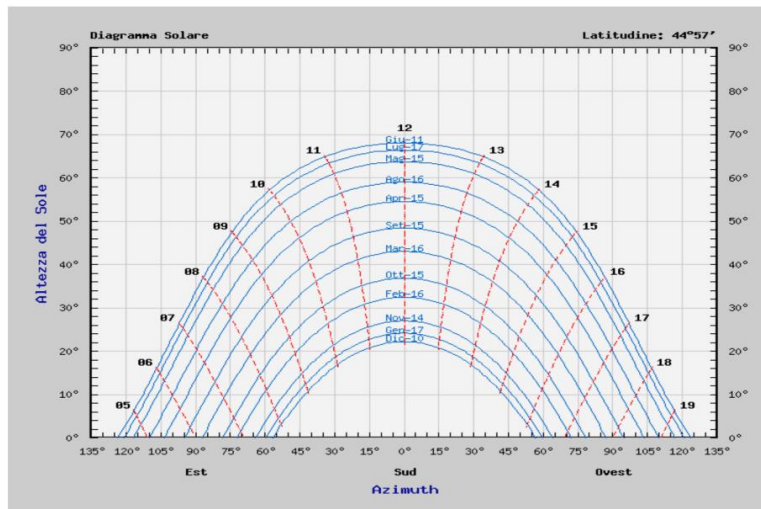


Figura 33: Cartesian solar diagram

Looking at the values in Table 5 and the corresponding graphs in Figures 34 (a) and Figure 34 (b), it can be seen that the months that correspond to higher sun elevation are also the months during which solar irradiation and energy production will be greatest.

Tabella 5: Daily irradiance and Producibile energy value

Month	kWh/m <sup>2</sup>	MJ/m <sup>2</sup>
Gen	1,26	4,53
Feb	2	7,20
Mar	3,44	12,37
Apr	4,6	16,56
May	5,59	20,14
Jun	6,38	22,98
Jul	6,56	23,62
Ago	5,6	20,14
Sept	4,2	15,11
Oct	2,43	8,74
Nov	1,33	4,79
Dec	1,06	3,81

It can also be observed, as was to be expected, that the months during which the sun has a lower path correspond in Figure 34 (a) and Figure 34 (b) to the months in which solar radiation and thus producible energy are lower. Thus, from this initial analysis of the installation location, it is expected that the middle months of the year will have higher energy production, lower self-consumption, and thus a higher amount of energy sold to the grid. While months such as January, February, October, November and December will have lower energy produced, higher self-consumption and consequently a lower share of quote sold to the grid.

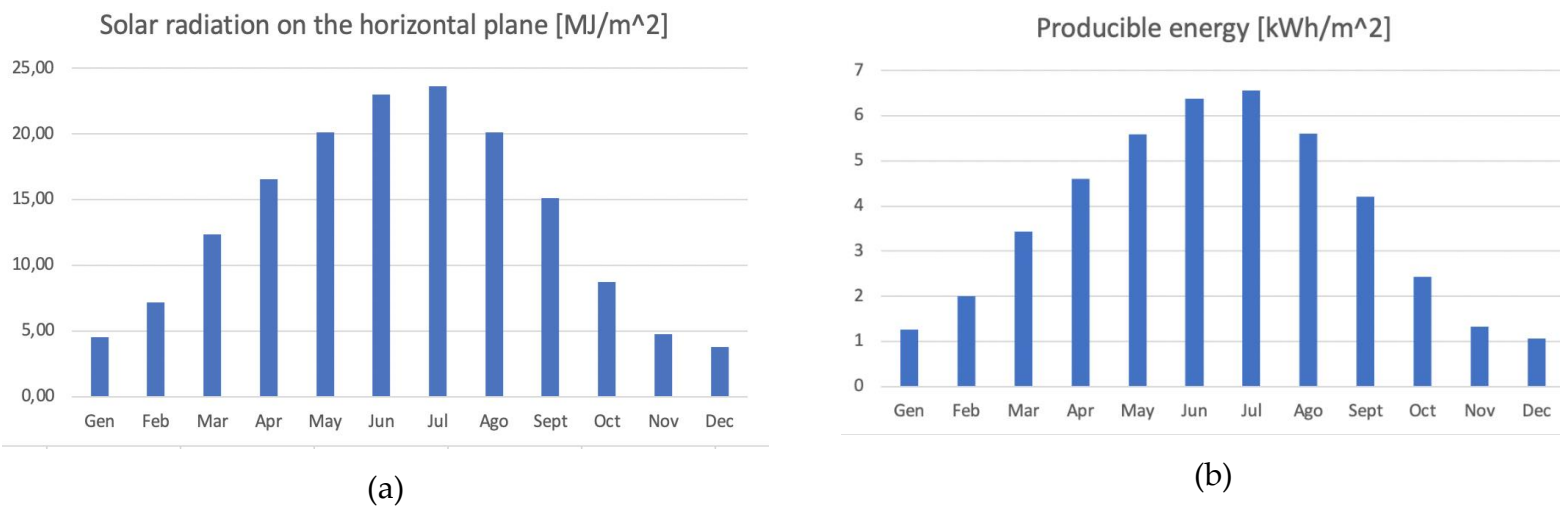


Figura 34 : (a) Solar radiation on the horizontal plane; (b) Producibile energy

### 2.2.1.3. Load Analysis

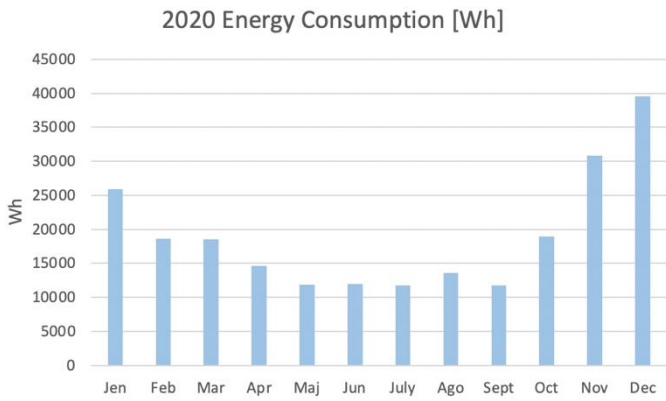
The building where the system will be installed is used for small farm machinery. Consumption for the years 2020 and 2021 is shown in Table 6, which is useful for making comparisons and forecasts.

The data that were provided by the owner are collected by months and divided into the three daily time slots: F1, F2 and F3. The F1 band is the so-called "rush hour" band, so it runs from 08:00 to 18:00; The F2 band is from 07:00 to 08:00 and then from 19:00 to 22:00; As for the F3 band, on the other hand, it goes from 8:00 pm to 06:00 am.

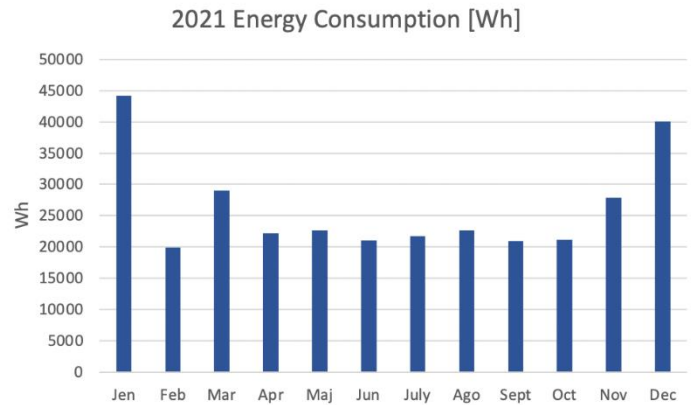
Tabella 6: Verdeto’s energy consumption

		IT001E54925975			
		F1	F2	F3	tot
		kWh	kWh	kWh	Wh
2020	Jen	8631	5852	11419	25902
2020	Feb	5609	5064	8010	18683
2020	Mar	5926	4346	8211	18483
2020	Apr	5652	3398	5582	14632
2020	Maj	4448	3168	4264	11880
2020	Jun	4609	3128	4254	11991
2020	July	4293	2954	4509	11756
2020	Ago	4395	3227	5947	13569
2020	Sept	4564	2915	4259	11738
2020	Oct	6886	5264	6841	18991
2020	Nov	10327	7719	12767	30813
2020	Dec	13307	8132	18082	39521
2021	Jen	13765	10588	19810	44163
2021	Feb	7149	4914	7837	19900
2021	Mar	9808	7430	11837	29075
2021	Apr	7635	5147	9435	22217
2021	Maj	7077	5084	10505	22666
2021	Jun	7057	4922	9014	20993
2021	July	7398	5476	8856	21730
2021	Ago	7452	5382	9763	22597
2021	Sept	6888	5315	8756	20959
2021	Oct	5992	5586	9571	21149
2021	Nov	8949	6547	12397	27893
2021	Dec	13026	8925	18138	40089

The data were collected from the POD having identification code IT001E54925975. Data from the table are shown in the following graphs in Figures 35 (a) and Figure 35 (b) for the year 2020 and 2021, respectively.



(a)



(b)

Figura 35: (a) 2020 Energy consumption; (b) 2021 Energy consumption

The first statement that can be made by looking at the two graphs is that the months during which electricity consumption is highest for both years are January, March, November and December (reaching peaks of almost 45kWh). While the middle months of the year, when temperatures are higher, there is lower electricity consumption, as might be expected. It is interesting to make the comparison of consumption between the year 2020 and the year 2021, shown in Figure 36.

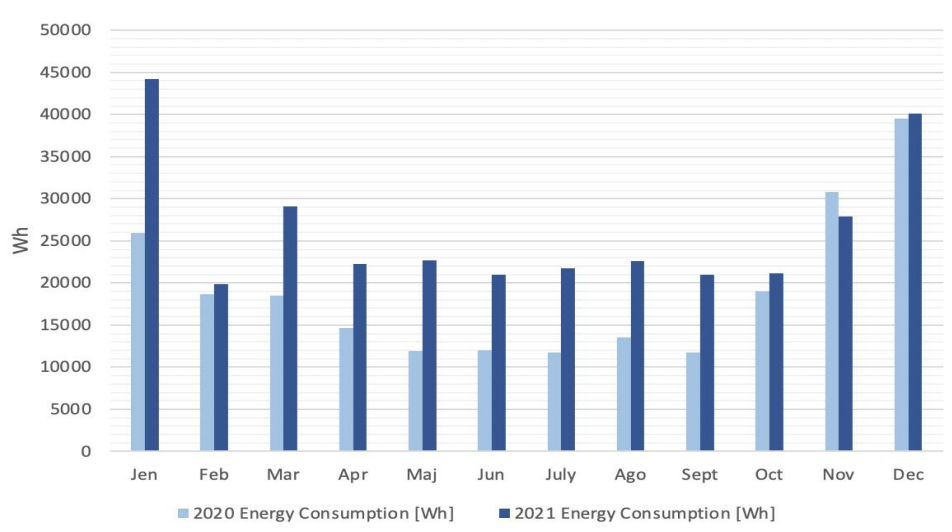


Figura 36: Energy consumption 2020 vs 2021

It can be seen from the graph how consumption in 2021 is significantly increased compared to consumption in 2020, this will allow for a higher share of self-consumption and a lower share of energy fed into the grid. In particular, the months that have had the greatest increase are the eight seven months of the year, thus including the middle months.

For the purpose of doing some practical analysis regarding the quote of energy consumed that will be produced by the PV system, it is useful to analyse in more detail the time slots during which the most electricity is consumed (F1, F2 and F3). This is because as we know, a photovoltaic system is capable of generating power on average from 6:00 a.m. until 6:00 p.m. at night. It can be seen in more detail the times when the system will produce by looking at the solar Cartesian graph in Figure 33.



Figura 37: (a),(b) Consumption distribution in hourly bands

As can be seen from the pie charts in Figure 37(a) and 37(b), the time slot during which there is the highest energy consumption is F3 (more than 40 percent), which corresponds to the time frame in which the PV system will not produce (as it runs from 8:00 p.m. to 6:00 a.m.). Then, more than 33 percent of consumption occurs during the F1 time frame, a time frame during which the PV system will produce the most electricity; therefore, the largest quote of self-consumption can be expected during this time frame. The remaining approximately 20% corresponds to the F2 band, during which the PV system will produce a modest amount of energy.

## 2.2.2. Technical Analysis of Verdeto photovoltaic plant

The following chapter will go into the technical details of the photovoltaic system components that were sized during the preliminary phase of the Verdeto project: modules, inverters and cables.

### 2.2.2.1. Modules and Substructures: generalities & technical analysis

The modules used in the Verdeto PV system are JA Solar Module 380W Mono PERC (JAM60S20-380/MR), the characteristics of which were analyzed in Section 1.2.3 as they are monocrystalline modules. The most important characteristic of these kind of modules is the half-cell technology with 9 busbars, together with shorter half-cell cells connected internally in two series of strings. It reduces current losses and increases performance even when the module is affected by partial shading. The mechanical diagram is shown in Figure 38.

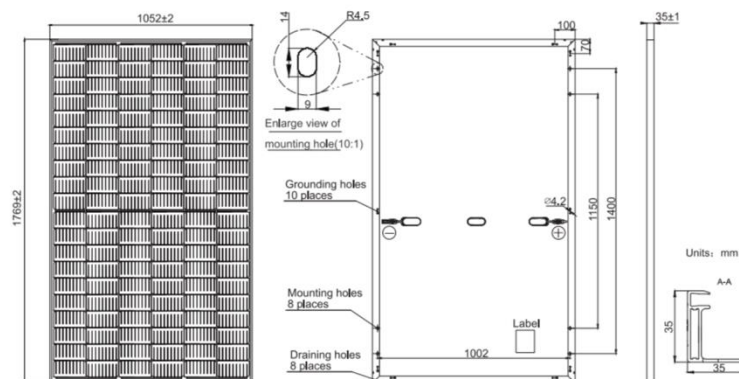


Figura 38: module technical diagram

The most relevant information is the lengths of the short side, long side, and module thickness, 1052mm, 1769mm, and 35mm, respectively. The module thickness is an important piece of information for selecting the clamps that will be used to attach the module to the substructure. It is also important for the structural calculation of substructures to point out that the module weight is 20.5Kg.



The main electrical parameters (Rated maximum power, open circuit voltage, short circuit current and module efficiency), which are useful for the actual sizing of a PV system, are shown in Table 7.

Tabella 7: Main modules' parameters

Electrical parameters at STC	
Pmax [W]	380
Voc [V]	41.62
Isc [A]	11.47
Module Efficiency [%]	20.4

Finally, Figure 39 (a),(b) and (c) shows the characteristic curves of the module used.

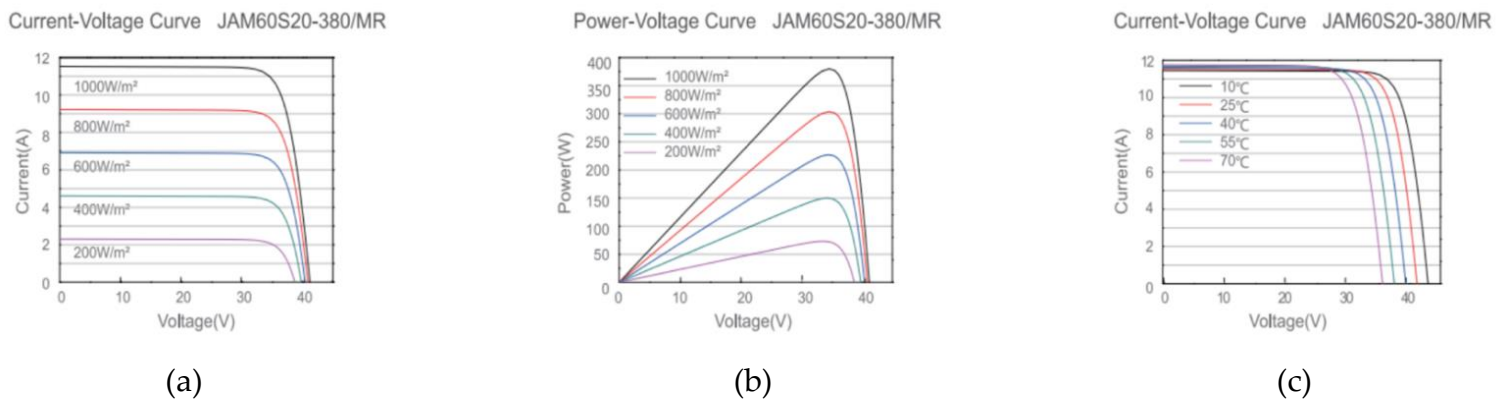


Figura 39: (a) Current- voltage curve; (b) Power-voltage curve; (c) Current-voltage curve

The electrical data above and the curves in Figure 39 will be critical in sizing the inverter and strings.

It is interesting to dwell on the type of substructure used. Since this will also influence the division of the modules into the different MPPTs of the inverters. As we have previously seen the plant is located on a flat roof, so it was decided to use an E/W substructure. Specifically, it was decided to use the Evo 2.0 EAST/WEST substructure provided by PMT. The main characteristics are listed in table 8.

Tabella 8: Main substructure's parameters

Bracket tilt $\alpha$ [°]:	10
Inter-row spacing a [mm]:	60
System variant:	Comfort
Friction Constant $\mu$	0.3
The default set-friction coefficient is 0.5 and checked by the installer / buyer (wet and dry test). If a lower friction coefficient is determined, it is mandatory to enter the value here, for the surcharge calculation! A higher value can be set to the maximum limit of 0.7 if it has been determined.	
Recommended distance to roof border [mm]:	556
User defined distance to roof border [mm]:	556
Cross brace only in corners:	No
Cross brace on edge:	No
Cross brace for low-resistance connection:	No
Use third rail:	No
Stone weight [kg]:	15 kg
Ballast clip on the edge:	Yes
Ballast clamp in the middle of the field:	Yes
Mechanical fastening:	No
Fastening against caterpillar effect:	No
Ballast trays used:	No
Maximum permissible weight per single module / double module:	0
Wind tunnel report:	MEW07-1-2

The structure of the EVO 2.0 with the main dimensional features is shown in Figure 40.

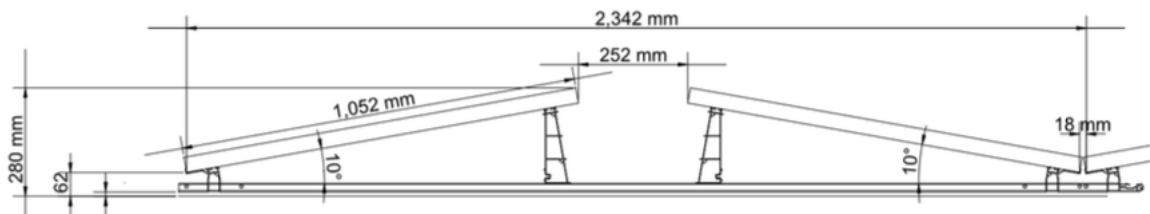


Figura 40: PMT EVO 2.0 E/W

Finally, based on the load parameters listed in Table 9, it was decided how to distribute the ballasts on the system

Tabella 9: Main substructure's load parameters

<b>Snow load</b>	1.29 kN/m <sup>2</sup>
<b>Wind load</b>	0.75 kN/m <sup>2</sup>
<b>Friction Constant <math>\mu</math></b>	0.3
<b>Factor of Safety for Uplift</b>	1.5
<b>Factor of Safety for Sliding</b>	1.5
<b>Load factor applied to Dead Load</b>	0.9
<b>Weight per ballast block</b>	15 kg
<b>Number of ballast blocks:</b>	104
<b>System surface area</b>	692.77 m <sup>2</sup>
<b>Roof area</b>	986.92 m <sup>2</sup>
<b>Total ballast weight</b>	1,560 kg
<b>Weight Module/Rack</b>	7,795.2 kg
<b>Total System weight</b>	9,355.2 kg
<b>Surface load on system area</b>	13.5 kg/m <sup>2</sup>
<b>Surface load on roof</b>	9.48 kg/m <sup>2</sup>
<b>Average horizontal load</b>	0.052 kN
<b>Maximum horizontal load</b>	0.066 kN
<b>Total horizontal load</b>	8.81 kN

Therefore, based on the constraints given by the load the structure can bear, snow load, wind load and other detail factors, it was decided to use 104 blocks of 15Kg each. Below, Figure 41 shows the ballasting distribution scheme of the entire facility.

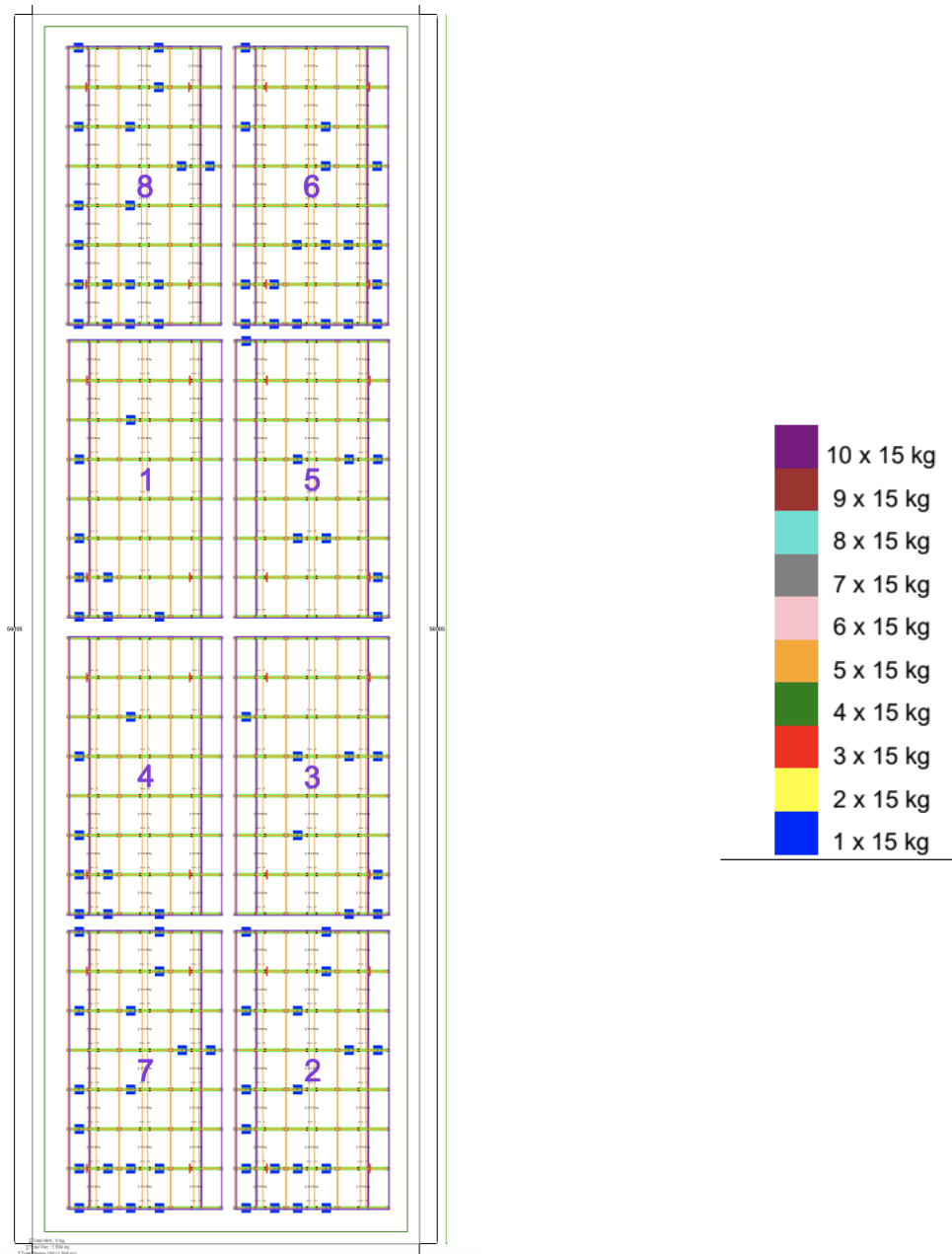


Figura 41: Ballast scheme

Let's now have a deeper technical look to the chosen modules in order to guarantee the correct sizing of the photovoltaic plant. Considering using monocrystalline silicon modules of unit power equal to 380 W, 336 modules would be required, a number that can be estimated by the relation  $127.68\text{kWp}/380=336$ .

Taking into consideration the string voltage (which influences the input voltage of the inverter) and the total current of the strings in parallel (which mainly influences the choice of cables), we choose to group the modules into 16 strings of 21 modules in series each, for a total of  $16 \times 21 = 336$  modules with a total maximum power output of  $336 \times 380 = 127.68$  kWp. The main characteristics of the generic module stated by the manufacturer and useful for calculations are summarized in Table 10. [13]

Tabella 10: Main modules parameters useful for sizing the PV plant

JAM60S20-380/MR	
Rated Power $P_{MPP}$	380W
Efficiency	20,40%
Rated Voltage $V_{MPP}$	35.05V
Rated current $I_{MPP}$	10.93A
Open-circuit voltage $V_{oc}$	41.62V
Short-circuit current $I_{sc}$	11.47A
Maximum voltage	1000V
Temperature coefficient $P_{MPP}$	-0.35 %/°C
Temperature coefficient U	-0.15 V/°C
Dimensions	1776x1052x35 mm
Area	1.87 $m^2$
Insulation	Class II

Thus, the total area covered by the modules will be  $1.87 \times 336 = 628.32m^2$ , which is less than the available area of the roof pitch, equal to  $993.054m^2$ .

Assuming minimum and maximum temperatures of the modules of  $-40^\circ\text{C}$  and  $+85^\circ\text{C}$  and taking into account that the temperature relative to standard test conditions is  $25^\circ\text{C}$ , we obtain with Equation (16) the voltage variation of a PV module, compared with standard conditions.

$$V(T)_{oc} = V_{oc,stc} - N_s \times \beta \times (25 - T_{cel}) \quad (16)$$

- Open-circuit maximum voltage:  $41.62 + 0.13 \times (25 + 40) = 47.57\text{V}$
- MPP minimum voltage:  $35.3 + 0.15 \times (25 - 80) = 27.05\text{V}$
- MPP maximum voltage:  $35.3 + 0.15 \times (25 + 40) = 45.05\text{V}$

Finally, the electrical characteristics of the strings are calculated: [14]

- MPP voltage:  $21 \times 34.77 = 741.37\text{V}$
- MPP current:  $21 \times 10.93 = 10.93\text{A}$
- Short-circuit maximum current:  $1.25 \times 10.93 = 13.66\text{A}$
- Open-circuit maximum voltage:  $21 \times 47.57\text{V} = 998\text{V}$
- MPP minimum voltage:  $21 \times 26.52 = 568.05\text{V}$
- MPP maximum voltage:  $21 \times 45.05 = 946\text{V}$

### 2.2.2.2. Inverters: generalities and technical analysis

The conversion unit consists of the static converters (Inverters).

The DC/AC converter used is suitable for transferring power from the PV array to the distributor's grid, in accordance with applicable technical and safety regulatory requirements. The input voltage and current values of this equipment are compatible with those of the respective PV array, while the output voltage and frequency values are compatible with those of the grid to which the system is connected.

The main characteristics of the conversion unit are:

- Forced-switching inverter with PWM (pulse-width modulation) technique, without clock and/or internal voltage or current references, assimilated as a "system not capable of sustaining voltage and frequency in the normal range," in accordance with the requirements for production systems in CEI 0-21 and equipped with MPPT (maximum power tracking) function
- DC-side input from photovoltaic generator manageable with ungrounded poles, i.e., IT system.
- Compliance with general standards on EMC and RF emission limitation: compliance with CEI 110-1, CEI 110-6, CEI 110-8 standards.
- Protections for disconnection from the grid for out-of-threshold values of grid voltage and frequency and for fault overcurrent in accordance with the requirements of CEI 0-21 standards and those specified by the local electric distributor. Automatic reset of protections to prepare for automatic startup.
- CE mark compliance.
- Degree of protection appropriate for location near the PV array (IP65).
- Declaration of product conformity with applicable technical regulations, issued by the manufacturer, with reference to type tests carried out on the component at a approved and recognized certification body.
- Input voltage range appropriate to the output voltage of the PV generator.
- Maximum efficiency  $\geq 90\%$  at 70% of rated power.

Tabella 11: Main inverters' characteristics

Inverter construction data	
Manufacturer	SMA TECHNOLOGIE
Serie	Sunny Tripower CORE1 STP 50-40_01
MPPT	6
Input per MPPT	2
Electrical characteristics	
Rated power	50 kW
Maximum power	51,1 kW
Maximum power per MPPT	8,5 kW
Rated voltage	800V
Maximum voltage	1000V
Minimum voltage per MPPT	150V
Maximum voltage per MPPT	1000V
Output Rated voltage	400 Vac
Rated current	120A
Maximum current	120A
Maximum current per MPPT	30A
Efficiency	0,98

The conversion unit consists of 3 inverters having characteristics summarized in the table 12 (a), (b) and (c)

Tabella 12: (a) Inverter 1 string configuration; (b) Inverter 2 string configuration; (c) Inverter 3 string configuration

Inverter 1	MPPT 1	MPPT 2	MPPT 3	MPPT 4	MPPT 5	MPPT 6
Moduli in serie:	21	21	21	21	21	0
Stringhe parallelo: <sup>in</sup>	1	1	1	1	1	1
Esposizioni:	Ovest	Ovest	Ovest	Ovest	Ovest	Ovest
Tensione di MPP (STC):	730,2 V	730,2 V	730,2 V	730,2 V	730,2 V	0 V
Numero moduli: <sup>di</sup>	21	21	21	21	21	0

(a)

Inverter 2	MPPT 1	MPPT 2	MPPT 3	MPPT 4	MPPT 5	MPPT 6
Moduli in serie:	21	21	21	21	21	0
Stringhe parallelo: <sup>in</sup>	1	1	1	1	1	1
Esposizioni:	Est	Est	Est	Est	Est	Est
Tensione di MPP (STC):	730,2 V	730,2 V	730,2 V	730,2 V	730,2 V	0 V
Numero moduli: <sup>di</sup>	21	21	21	21	21	0

(b)

Inverter 3	MPPT 1	MPPT 2	MPPT 3	MPPT 4	MPPT 5	MPPT 6
Moduli in serie:	21	21	21	21	21	21
Stringhe parallelo:	1	1	1	1	1	1
Esposizioni:	Ovest	Ovest	Ovest	Est	Est	Est
Tensione di MPP (STC):	730,2 V	730,2 V	730,2 V	730,2 V	730,2 V	730,2 V
Numero di moduli:	21	21	21	21	21	21

(c)

We choose to install 3 three-phase inverters of 50kW rated input power each; therefore, two inverters will have 5 strings in parallel, while only one will have 6 strings in parallel, as was seen in the previous paragraph. The three-phase inverters chosen will perform DC to AC conversion with PWM technique and IGBT bridging. They have input and output filters for suppression of both conducted and radiated emitted noise and a sensor of isolation to ground of the PV modules. They are equipped with the tracking device of the point of maximum power MPPT and have a protection internally to prevent the feeding of currents into the grid with continuous components. Technical characteristics of the inverter are summarized in Table 11.

For verification of proper string-inverter coupling it is first necessary to verify that the maximum no-load voltage at the ends of the string is lower than the maximum input voltage supported by the inverter: [13]

$$998 < 1000 \quad OK$$

In addition, the minimum MPP voltage of the string must not be less than the minimum MPPT voltage of the inverter:

$$568.05 > 500 \quad OK$$

While the maximum MPP voltage of the string must not be higher than the maximum MPPT voltage of the inverter:

$$946 < 950 \quad OK$$

Finally, the total maximum short-circuit current of the 6 strings connected in parallel and pertaining to each inverter must not exceed the maximum input current that the inverter can withstand:

$$6 \times 13.66 = 81.96A < 120 \quad OK$$



2.2.2.3. Cables: generalities & technical analysis

The modules are connected to each other in series through cable H1Z2Z2-K and each resulting string is connected to the field switchboard, inside the shed immediately upstream of the inverter, through solar cables of length L=1m placed in 2 channels containing 6 bundled circuits.

The characteristics of the solar cables are summarized in Table 13.

Tabella 13: Main cables' characteristics

Solar Cable H1Z2Z2-K	
Section	6 mm <sup>2</sup>
Rated voltage U <sub>0</sub> /U	AC: 1000/1000V
	DC: 1500/1500V
Working temperature	-40°C up to+ 90°C
Current carrying capacity in air	70A
De-rating factor of capacity at 70°C	0.91
Maximum conductor temperature	120°C

The flow rate I<sub>z</sub> of solar cables in the condition of laying in pipe in bundle at the operating temperature of 70°C results to be equal to Equation (17).

$$I_z = 0.57 \times 0.9 \times 0.91 \times I_0 = 32.68A \tag{17}$$

Where 0.9 represents the correction factor for pipe laying or channel of solar cables, while 0.57 is the correction factor for laying in bundle of 6 circuits.

Looking at Equation (18) the capacity is found to be greater than the short-circuit current maximum circuit current of the string.

$$I_z > 1.25 \times I_{sc} = 14.34A \tag{18}$$

The module frames and support structure of each string are grounded with a 6 mm<sup>2</sup> yellow-green N07V-K cable.

The connection between the inverter and the inverter parallel switchboard is made with 3 single-core FG16OR16 G16TOP 16 mm<sup>2</sup> cables of length L=1m laid in protective tube of capacity equal to 69A, which is greater than the rated output current of the 3 phase inverter, as it is observable in Equation (19).

$$I_z > \frac{P_n}{\sqrt{3} \times V_n \times \cos\phi_n} = 36.44A \tag{19}$$

Connections between inverter parallel switchboard and produced energy meter (length L=3m), between meter and general switchboard of the company (length L=7m) are made for the phases with 3 single-core FG16OR16 of 50mm<sup>2</sup> cables laid in

protective tube of capacity equal to 110A, Equation (20) shows that it is greater than the rated output current of the PV system. [13]

$$I_z > \frac{P_n}{\sqrt{3} \times V_n \times \cos\varphi_n} = 109.32A \quad (20)$$

### 2.2.3. Productivity Simulation

The two software applications SunnyDesign and PVsyst are used in this chapter to analyse the two simulations that were performed at the preliminary stage. In both simulation programmes, the system is first described, and then the results of the producibility tests are examined. The significant differences between the two software will then be covered in the following chapter.

It is important to note that manual cable sizing is not supported by SunnyDesign software, just as detailed losses like cable/module ageing losses, dirt losses, module quality losses, mismatch losses, PV loss due to irradiance level, PV loss due to temperature, and other kinds of losses that PVsyst investigates are not supported either.

#### 2.2.3.1. SunnyDesign Software Productivity Simulation

SunnyDesign is software used for the analysis of photovoltaic systems of all kinds and is owned by SMA Technology. It is a very malleable and easy-to-use software that allows one to have at the preliminary stage a clear, albeit approximate, view of the producibility that the PV plant will have.

This software makes it very easy to select the components to be used in the system. The configuration chosen for the first of the three inverters is shown in Figure 42.

1 x SMA STP 50-40/41 (CORE1) (PV system section 1)	
Peak power:	39.90 kWp
Total number of PV modules:	105
Number of PV inverters:	1
Max. DC power (cos φ = 1):	51.00 kW
Max. AC active power (cos φ = 1):	50.00 kW
Grid voltage:	20.0 kV
Nominal power ratio:	128 %
Dimensioning factor:	79.8 %
Displacement power factor cos φ:	1
Full load hours:	813.4 h




Figura 42: Inverter 1 configuration

As it is visible in Inverter 1 105 modules, divided in 5 strings are connected, for an amount of peak power of 39.90kW. Doing so ensures that the maximum DC input power and maximum DC output power are met.

In fact, as can be seen in Figure 42, the sizing factor is 79.8 percent. The software also allows you to view the input arrays distributed over the 6 MPPTs, as shown in Figure 43. As was seen earlier, five strings are connected to this inverter, each having 21 modules and therefore five of the six MPPTs will be used, each with a single input

string. Interestingly, it was decided at the design stage to configure inverter 1 with only strings having modules facing east.

PV design data	
<b>Input A: East Array</b>	21 x Shanghai JA Solar Technology Co. Ltd. JAM60S20-380/MR (1500V) (02/2021), Azimuth angle: -50 °, Tilt angle: 10 °, Mounting type: Roof
<b>Input B: East Array</b>	21 x Shanghai JA Solar Technology Co. Ltd. JAM60S20-380/MR (1500V) (02/2021), Azimuth angle: -50 °, Tilt angle: 10 °, Mounting type: Roof
<b>Input C: East Array</b>	21 x Shanghai JA Solar Technology Co. Ltd. JAM60S20-380/MR (1500V) (02/2021), Azimuth angle: -50 °, Tilt angle: 10 °, Mounting type: Roof
<b>Input D: East Array</b>	21 x Shanghai JA Solar Technology Co. Ltd. JAM60S20-380/MR (1500V) (02/2021), Azimuth angle: -50 °, Tilt angle: 10 °, Mounting type: Roof
<b>Input E: East Array</b>	21 x Shanghai JA Solar Technology Co. Ltd. JAM60S20-380/MR (1500V) (02/2021), Azimuth angle: -50 °, Tilt angle: 10 °, Mounting type: Roof

Figura 43: Inverter 1 MPPTs configuration

SunnyDesign also makes it possible to verify that the plant sizing carried out at the preliminary stage is adhered to. Figure 44 shows the check that the software performs.

	Input A:	Input B:	Input C:
Number of strings:	1	1	1
PV modules:	21	21	21
Peak power (input):	7.98 kWp	7.98 kWp	7.98 kWp
Inverter min. DC voltage (Grid voltage 20.0 kV):	150 V	150 V	150 V
PV typical voltage:	✓ 666 V	✓ 666 V	✓ 666 V
Min. PV voltage:	630 V	630 V	630 V
Max. DC voltage (Inverter):	1000 V	1000 V	1000 V
Max. PV voltage	✓ 946 V	✓ 946 V	✓ 946 V
Inverter max. operating input current per MPPT:	20 A	20 A	20 A
Max. MPP current of PV array:	✓ 10.9 A	✓ 10.9 A	✓ 10.9 A
Inverter max. input short-circuit current per MPPT:	30 A	30 A	30 A
PV max. circuit current	✓ 11.5 A	✓ 11.5 A	✓ 11.5 A
	Input D:	Input E:	Input F:
Number of strings:	1	1	---
PV modules:	21	21	---
Peak power (input):	7.98 kWp	7.98 kWp	---
Inverter min. DC voltage (Grid voltage 20.0 kV):	150 V	150 V	150 V
PV typical voltage:	✓ 666 V	✓ 666 V	---
Min. PV voltage:	630 V	630 V	---
Max. DC voltage (Inverter):	1000 V	1000 V	1000 V
Max. PV voltage	✓ 946 V	✓ 946 V	---
Inverter max. operating input current per MPPT:	20 A	20 A	20 A
Max. MPP current of PV array:	✓ 10.9 A	✓ 10.9 A	---
Inverter max. input short-circuit current per MPPT:	30 A	30 A	30 A
PV max. circuit current	✓ 11.5 A	✓ 11.5 A	---

Figura 44: Inverter 1 sizing check

For each of the five used inputs of the inverter, the main electrical quantities are verified. In fact, it is confirmed that the typical and maximum voltage of each array is within the limits of each MPPT (1000V). It is interesting to note the difference that exists between the typical string voltage in Figure 44 and the string voltage in Table

13(a). This difference is due to the fact that SunnyDesign estimates what the ordinary operating voltage of the inverter is based on solar irradiance, whereas in Table 13(a) you have the rated voltage value of the string. It is also verified that the current in normal operation and the short-circuit current of each string does not exceed the limits of the inverter.

Similar reasoning applies to Inverter 2, which has the same configuration as Inverter 1, the only difference being that the modules in each string face west. For the sake of completeness, the configuration of the inverter is shown in Figure 45, the configuration of each MPPT of the inverter in Figure 46, and finally in Figure 47 the verification of the correct sizing carried out at the preliminary stage.

1 x SMA STP 50-40/41 (CORE1) (PV system section 2)	
Peak power:	39.90 kWp
Total number of PV modules:	105
Number of PV inverters:	1
Max. DC power (cos φ = 1):	51.00 kW
Max. AC active power (cos φ = 1):	50.00 kW
Grid voltage:	20.0 kV
Nominal power ratio:	128 %
Dimensioning factor:	79.8 %
Displacement power factor cos φ:	1
Full load hours:	746.0 h




Figura 45: Inverter 2 configuration

Looking at the data in Figure 45, it can be seen that there is a decrease in inverter full load hours during the year. This result is a consequence of the different solar irradiance between east-facing and west-facing modules.

PV design data	
<b>Input A: West Array</b>	21 x Shanghai JA Solar Technology Co. Ltd. JAM60S20-380/MR (1500V) (02/2021), Azimuth angle: 130 °, Tilt angle: 10 °, Mounting type: Roof
<b>Input B: West Array</b>	21 x Shanghai JA Solar Technology Co. Ltd. JAM60S20-380/MR (1500V) (02/2021), Azimuth angle: 130 °, Tilt angle: 10 °, Mounting type: Roof
<b>Input C: West Array</b>	21 x Shanghai JA Solar Technology Co. Ltd. JAM60S20-380/MR (1500V) (02/2021), Azimuth angle: 130 °, Tilt angle: 10 °, Mounting type: Roof
<b>Input D: West Array</b>	21 x Shanghai JA Solar Technology Co. Ltd. JAM60S20-380/MR (1500V) (02/2021), Azimuth angle: 130 °, Tilt angle: 10 °, Mounting type: Roof
<b>Input E: West Array</b>	21 x Shanghai JA Solar Technology Co. Ltd. JAM60S20-380/MR (1500V) (02/2021), Azimuth angle: 130 °, Tilt angle: 10 °, Mounting type: Roof

Figura 46: Inverter 2 MPPTs configuration

	Input A:	Input B:	Input C:
Number of strings:	1	1	1
PV modules:	21	21	21
Peak power (input):	7.98 kWp	7.98 kWp	7.98 kWp
Inverter min. DC voltage (Grid voltage 20.0 kV):	150 V	150 V	150 V
PV typical voltage:	✓ 666 V	✓ 666 V	✓ 666 V
Min. PV voltage:	630 V	630 V	630 V
Max. DC voltage (Inverter):	1000 V	1000 V	1000 V
Max. PV voltage	✓ 946 V	✓ 946 V	✓ 946 V
Inverter max. operating input current per MPPT:	20 A	20 A	20 A
Max. MPP current of PV array:	✓ 10.2 A	✓ 10.2 A	✓ 10.2 A
Inverter max. input short-circuit current per MPPT:	30 A	30 A	30 A
PV max. circuit current	✓ 10.8 A	✓ 10.8 A	✓ 10.8 A

	Input D:	Input E:	Input F:
Number of strings:	1	1	
PV modules:	21	21	
Peak power (input):	7.98 kWp	7.98 kWp	---
Inverter min. DC voltage (Grid voltage 20.0 kV):	150 V	150 V	150 V
PV typical voltage:	✓ 666 V	✓ 666 V	---
Min. PV voltage:	630 V	630 V	---
Max. DC voltage (Inverter):	1000 V	1000 V	1000 V
Max. PV voltage	✓ 946 V	✓ 946 V	---
Inverter max. operating input current per MPPT:	20 A	20 A	20 A
Max. MPP current of PV array:	✓ 10.2 A	✓ 10.2 A	---
Inverter max. input short-circuit current per MPPT:	30 A	30 A	30 A
PV max. circuit current	✓ 10.8 A	✓ 10.8 A	---

Figura 47: Inverter 2 sizing verification

As expected, since the west-facing strings are also exposed to lower solar irradiance, the correct sizing of inverter 2 is verified.

Finally, data related to inverter 3, which has all six available MPPTs in use, is analyzed. Thus, there are 6 strings of 21 modules each, for a total of 126 modules. Unlike the other two inverters, the third inverter has 3 strings with modules facing east and 3 strings with modules facing west.

<b>1 x SMA STP 50-40/41 (CORE1) (PV system section 3)</b>	
Peak power:	47.88 kWp
Total number of PV modules:	126
Number of PV inverters:	1
Max. DC power (cos φ = 1):	51.00 kW
Max. AC active power (cos φ = 1):	50.00 kW
Grid voltage:	20.0 kV
Nominal power ratio:	107 %
Dimensioning factor:	95.8 %
Displacement power factor cos φ:	1
Full load hours:	936.2 h



Figura 48: Inverter 3 configuration

For the chosen configuration of the inverter, visible in Figure 48, the sizing factor is 95.8%, and the hours of use at full load obviously increase compared to Inverter 1 and Inverter 2, having strings facing east and strings facing west. The configuration of the inverter MPPTs is also shown in Figure 49 for completeness. In this case, MPPT E also has a string input.

	Input A:	Input B:	Input C:
Number of strings:	1	1	1
PV modules:	21	21	21
Peak power (input):	7.98 kWp	7.98 kWp	7.98 kWp
Inverter min. DC voltage (Grid voltage 20.0 kV):	150 V	150 V	150 V
PV typical voltage:	✓ 666 V	✓ 666 V	✓ 666 V
Min. PV voltage:	630 V	630 V	630 V
Max. DC voltage (Inverter):	1000 V	1000 V	1000 V
Max. PV voltage	✓ 946 V	✓ 946 V	✓ 946 V
Inverter max. operating input current per MPPT:	20 A	20 A	20 A
Max. MPP current of PV array:	✓ 10.9 A	✓ 10.9 A	✓ 10.9 A
Inverter max. input short-circuit current per MPPT:	30 A	30 A	30 A
PV max. circuit current	✓ 11.5 A	✓ 11.5 A	✓ 11.5 A
	Input D:	Input E:	Input F:
Number of strings:	1	1	1
PV modules:	21	21	21
Peak power (input):	7.98 kWp	7.98 kWp	7.98 kWp
Inverter min. DC voltage (Grid voltage 20.0 kV):	150 V	150 V	150 V
PV typical voltage:	✓ 666 V	✓ 666 V	✓ 666 V
Min. PV voltage:	630 V	630 V	630 V
Max. DC voltage (Inverter):	1000 V	1000 V	1000 V
Max. PV voltage	✓ 946 V	✓ 946 V	✓ 946 V
Inverter max. operating input current per MPPT:	20 A	20 A	20 A
Max. MPP current of PV array:	✓ 10.2 A	✓ 10.2 A	✓ 10.2 A
Inverter max. input short-circuit current per MPPT:	30 A	30 A	30 A
PV max. circuit current	✓ 10.8 A	✓ 10.8 A	✓ 10.8 A

Figura 49: Inverter 3 sizing verification

As expected, although the inverter has an extra string input, the sizing is verified as in the first two cases, since each string always has 21 modules connected in series.

SunnyDesign is approximate software, so it does not allow accurate cable sizing, but only allows you to enter the distance (70m) to the medium-voltage substation, after which it independently verifies losses and provides results that will be discussed below in Figure 50.

Month	Energy yield [kWh]	Self-consumption [kWh]	Grid feed-in [kWh]	Purchased electricity [kWh]
1	3553 (2.8 %)	3384	169	25734
2	5788 (4.6 %)	5021	767	21277
3	10926 (8.8 %)	7948	2979	20140
4	13420 (10.8 %)	9172	4248	16253
5	16304 (13.1 %)	10248	6056	14774
6	16767 (13.5 %)	10664	6103	12491
7	18488 (14.8 %)	11559	6929	12430
8	16071 (12.9 %)	10364	5707	13621
9	10577 (8.5 %)	7870	2707	16488
10	6618 (5.3 %)	5735	883	20538
11	3473 (2.8 %)	3258	215	24920
12	2797 (2.2 %)	2789	9	26324

Figura 50: SunnyDesign simulation results

As previously mentioned, SunnyDesign is a very simple and intuitive software, as are the results it delivers.

The annual gran total, useful for further calculations, is summarized in Table 14.

Tabella 14: Annual results

Gran total	Energy yield [kWh]	Self-Consumption [kWh]	Grid feed-in [kWh]	Purchased electricity [kWh]
2021	125000	88010	36771	225000

Detailed analysis of the results reveals, as anticipated, that January, February, November, and December are the months with the lowest productivity and highest grid energy purchases. These are also the months when the least amount of energy will be injected into the power distribution network because they are the months with the lowest energy production. The results of the software show that the plant only produces 12.4% of the energy produced throughout the entire year, which the software calculated to be 124,782kWh (set as 100%) power, during these four months.

The months of April, May, June, July, and August are those in which the most energy is generated. An estimated 81,050kWh of energy will be produced during these months, or 65% of the annual total. The months of March, September, and October account for the remaining 22.5% of energy production.

As a result of what has been said above, it is evident that the middle months of the year will be those during which more energy is fed into the grid and consequently less energy is absorbed from it. On the other hand, during the early and late months of the year it will be necessary to draw a greater proportion of energy from the grid to allow the load to operate properly.

Finally, the distribution graph of energy produced during the simulation year is shown in Figure 51.

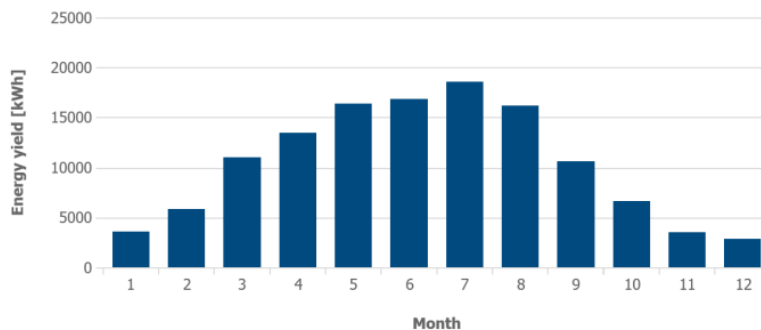


Figura 51: Energy yield per month



As a result of the installation of the photovoltaic system, it is interesting to conduct further analysis on the share of self-consumption and the share of self-sufficiency attained. Thus, the annual total equals 313MWh when taking into account the load consumption along 2021, as displayed in Table 7. In light of the information in Table 14, if the installation produces 125 MWh of total annual output, of which 88.010 MWh were self-consumed, this yields a self-sufficiency share of 28.1%. Additionally, the self-consumption share, which is equal to the discrepancy between the energy produced and the energy consumed by oneself, is 70.5%. The remaining 28.5%, or 36,771MWh, represents the energy that was fed into the grid.

The summary of the results is shown in Figure 52

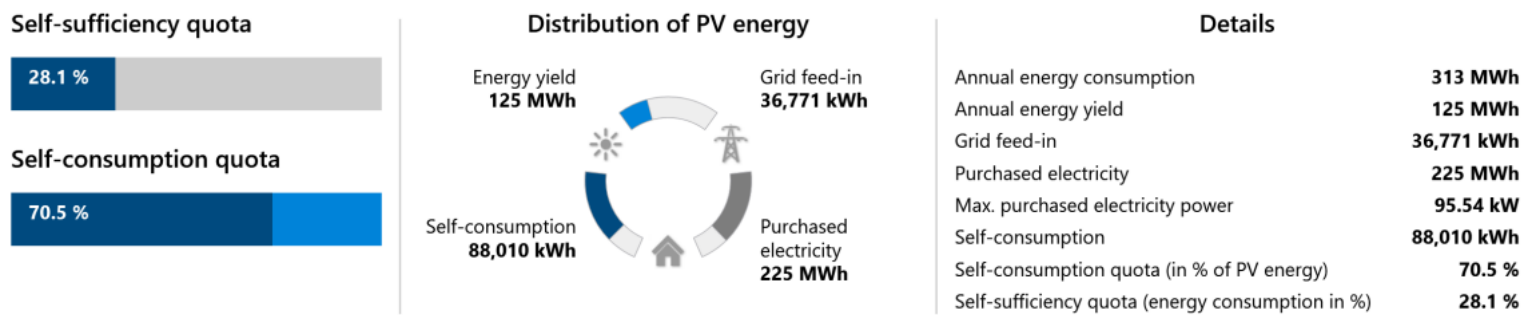


Figura 52: SunnyDesign results summary

### 2.2.3.2. PVsyst software productivity simulation

The simulation that was produced using the PVsyst programme is covered in the following chapter. This software enables a considerably more thorough and precise analysis than the previous one, in part because it enables the detailed entry of the monthly load consumption shown in Table 6 as well as the consideration of all the system's specific losses. As with the SunnyDesign software, the system will first be detailed, followed by a thorough analysis of all plant losses, and then a discussion of the findings.

The photovoltaic plant, as seen in earlier chapters, has two orientations: 138 modules with a tilt angle of 10° and an azimuth of -50° (facing east), and another 138 modules with a tilt angle of 10° and an azimuth of 130° (facing west). The load's monthly energy consumption is also displayed in the general area, as seen in Figure 53.

**General parameters**

<b>Grid-Connected System</b>				<b>No 3D scene defined, no shadings</b>									
<b>PV Field Orientation</b>				<b>Sheds configuration</b>					<b>Models used</b>				
<b>Orientation</b>				No 3D scene defined					Transposition Perez				
Fixed planes	2 orientations								Diffuse Perez, Meteonorm				
Tilts/azimuths	10 / -50 °								Circumsolar separate				
	10 / 130 °												
<b>Horizon</b>				<b>Near Shadings</b>					<b>User's needs</b>				
Average Height 5.5 °				No Shadings					Monthly values				

Jan.	Feb.	Mar.	Apr.	May	June	July	Aug.	Sep.	Oct.	Nov.	Dec.	Year	
44.2	19.9	29.1	22.2	22.7	21.0	21.7	22.6	21.0	21.1	27.9	40.1	313	MWh/mth

Figura 53: general parameters of the photovoltaic plant

In Figure 54, a summary of the characteristics of the arrays input to each MPPT of the inverter can be seen. As has already been seen, you have 336 modules divided into 16 strings of 21 modules each. The three inverters used are rated at 50kWac, for a total of 150kWac. Since the system has a peak power of 128kW, the nominal DC/AC ratio is 0.85. For the calculation of losses, it is useful to note that the total area of the modules is 628 m<sup>2</sup>.

**PV Array Characteristics**

<b>PV module</b>		<b>Inverter</b>	
Manufacturer	JA solar	Manufacturer	SMA
Model	JAM60-S20-380-MR	Model	Sunny Tripower STP50-40-Core1
(Original PVsyst database)		(Original PVsyst database)	
Unit Nom. Power	380 Wp	Unit Nom. Power	50.0 kWac
Number of PV modules	336 units	Number of inverters	3 units
Nominal (STC)	128 kWp	Total power	150 kWac
Modules	16 Strings x 21 In series	Operating voltage	188-800 V
<b>At operating cond. (50°C)</b>		Pnom ratio (DC:AC)	
Pmpp	116 kWp	0.85	
U mpp	664 V		
I mpp	175 A		
<b>Total PV power</b>		<b>Total inverter power</b>	
Nominal (STC)	128 kWp	Total power	150 kWac
Total	336 modules	Number of inverters	3 units
Module area	628 m <sup>2</sup>	Pnom ratio	0.85

Figura 54: photovoltaic array characteristics

Since the system has already been analysed in detail previously, as well as the correct sizing and coupling between the different components has already been verified, the losses that PVsyst allows for are now analyzed in detail. Let's start with the losses related to Global Horizontal Irradiation, shown in Figure 54.

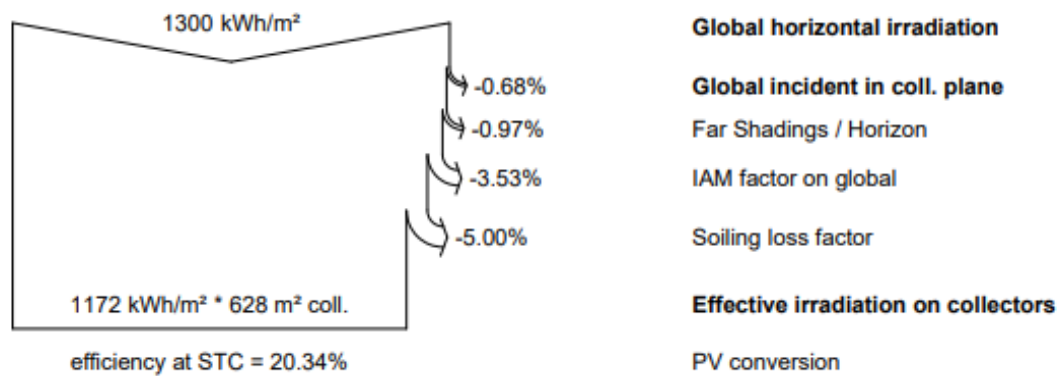


Figura 55: Global horizontal irradiation losses

Starting from a global horizontal irradiation of 1300kWh/m<sup>2</sup> the losses correlated are:

- Global incident in collateral plane losses: it is merely the outcome of the irradiance being transposed from horizontal to the array's plane, and it corresponds to 0.68%
- Far shadings/Horizon losses: In order to develop a profile of the surrounding landscape, PVsyst gathers over 1 million elevation data from the neighbourhood whenever an irradiance map or performance simulation is run. Horizon profiles are the resulting 360-degree elevation maps. The specific horizon profile for the two orientations is shown in figure 56, the shading areas due to the profile are therefore visible, these result in a loss of 0.97%.

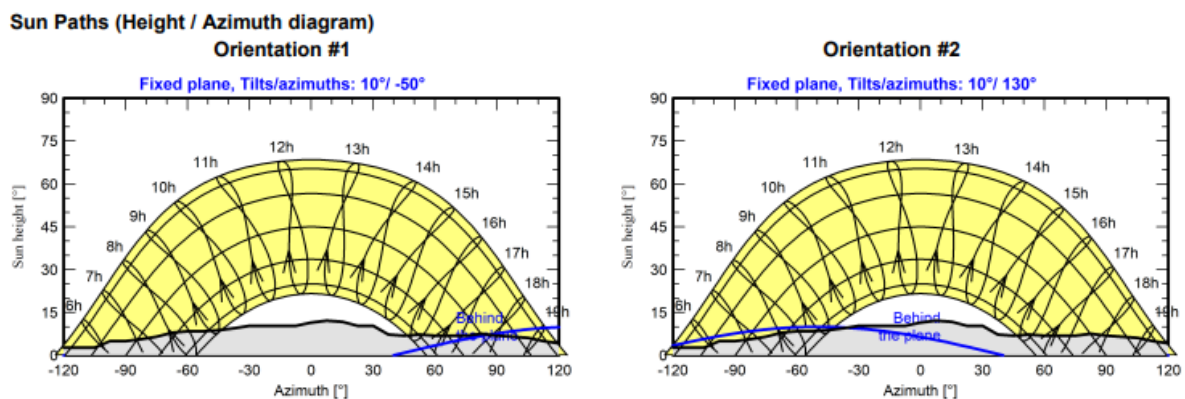


Figura 56: Horizon profile

- IAM factor on global losses: The incidence effect (also known as IAM, or "Incidence Angle Modifier") is the reduction of the amount of light that actually reaches the surface of the photovoltaic cells as compared to the incidence under normal incidence. Reflexions on the glass cover, which rise with the incidence angle, are the principal cause of this decline. This kind of loss corresponds to a decrease of 3.53%.
- Soiling loss factor: The buildup of dirt and how it affects the system's function is an unpredictability that is highly dependent on the system's surroundings,

such as the weather. This is typically modest and may be disregarded (less than 1%) in residential areas and medium-rainy regions (like the centre of Europe). It could be crucial for some seasonal operations in rural areas with agricultural activity. The bottom cells are partially shaded and tend to retain more dust due to the buildup of dusts and the development of mosses and lichens along the frame of the modules. Furthermore, rain does not clean up these pollutants. It is advised to use frameless modules whenever possible with modest tilts. Bird droppings pose a severe issue because rainy weather typically does not wash them away. Of course, the rainfall has a significant impact on the soiling losses. Because the Verdeto PV plant is located in a rural area and is used for agricultural purposes, the estimated losses are 5% and correspond to losses due to soil/dust accumulation and losses due to dirt from the presence of birds.

Downstream of these losses, going from a global irradiation of  $1300 \text{ kWh/m}^2$  it results to an effective irradiation at the collectors of  $1172 \text{ kWh/m}^2$ . Multiplying by the total area of the modules, equal to  $628 \text{ m}^2$ , and by the efficiency in the standard condition of the modules, equal to 20.34%, gives the array nominal energy, equal to 149.6 MWh.

To the losses calculated previously, losses due to the modules are now added, shown in Figure 57. [15]

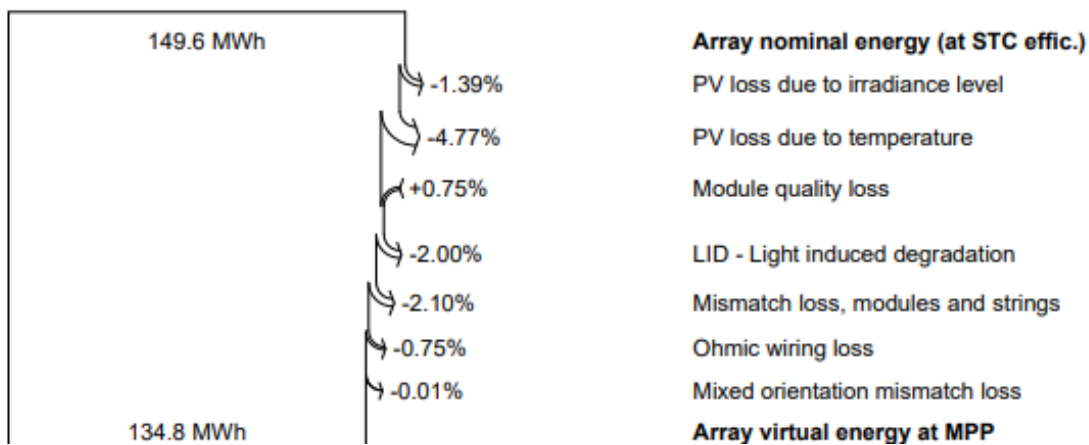


Figura 57: Array losses

Starting from an array nominal energy at STC efficiency of 149.6MWh the following source of losses are considered:

- PV loss due to irradiance level: Lower irradiances cause a module's efficiency to drop, resulting in "Irradiance loss" (in relation to  $1000 \text{ W/m}^2$ ). As a result, this irradiance loss is a result of the "one-diode" model's description of the inherent behaviour of the PV modules. This loss corresponds to 1.39%.
- PV loss due to temperature: Standard test conditions are specified for a cell temperature of  $25^\circ \text{ C}$ , but modules usually operate at temperatures higher. Thermal loss is calculated following the one-diode model. For crystalline silicon cells, the power loss is about  $-0,3\%/\text{C}$  at MPP. Temperature mainly affects the

voltage of the I(U) curve. Considering 16 MPP in use, we have a total loss equal to 4.8%. Shown in the Figure 58 are the I(U) curves at different temperature values available in the details of JA Solar's 380W module in PVSyst.

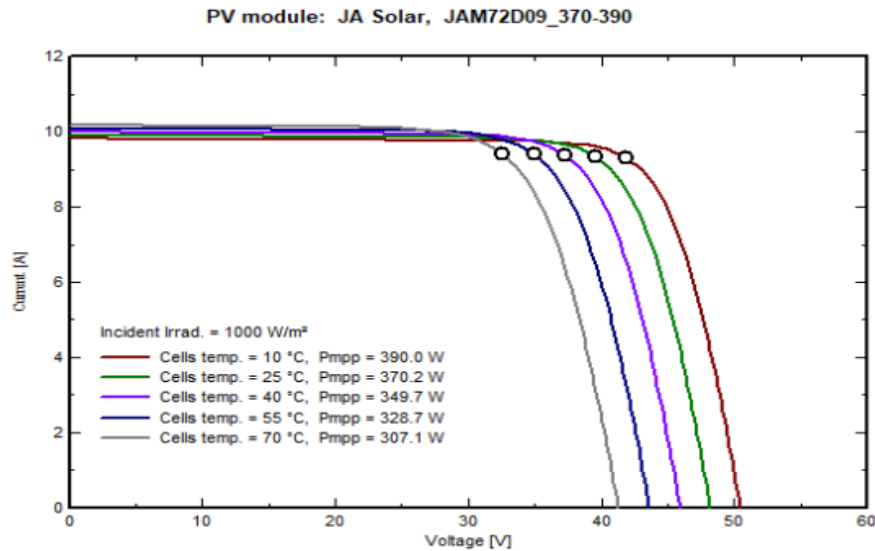


Figura 58: I(U) curves at different temperature

- **Module quality loss:** The Module Quality Loss parameter should reflect your level of assurance in the performance of the actual module in relation to the manufacturer's requirements. By default, PVSyst initialises the "Module Quality Loss" in accordance with the tolerance guidelines established by the PV module manufacturer. A quarter of the difference between these numbers will be chosen by PVSyst. For instance, it will be 1.5% with -3...+3% and -0.75% with positive sorting 0...+3%. (i.e. a negative loss value, representing a gain). When taking into account JAM60S20-380M/R, these losses translate into an increase of +0.75%.
- **Light induced degradation:** With crystalline modules, LID (Light Induced Degradation) is a performance decrease that occurs within the first few hours of exposure to the sun. It might specifically have an impact on the actual performance in comparison to the results of the factory flash testing that some PV module suppliers give. The LID loss, which may range from 1% to 3% depending on the wafer fabrication quality (or even more). Considering JAM60S20-380M/R modules, there is a loss of 2%. This value can be observed in the Figure 59 at point 1 on the x-axis, which corresponds to the time of first exposure of the module to sunlight. The graph can be found in the manufacturer's datasheet.

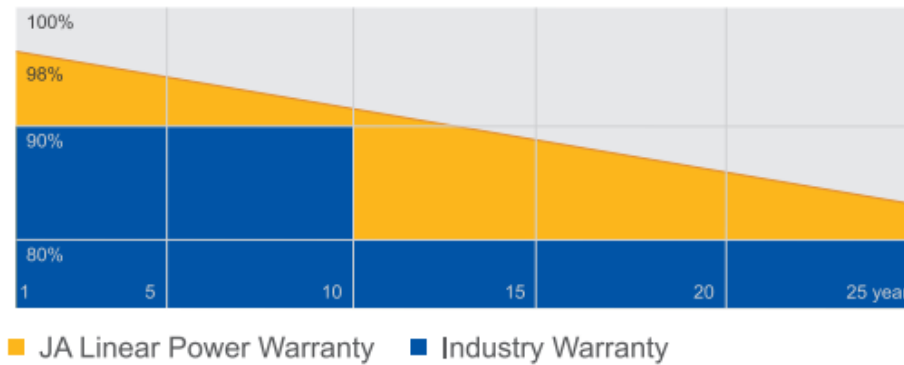


Figura 59: Warranty graph provided by manufacturer

- Mismatch loss: The "Mismatch loss" is mostly caused by the fact that the lowest current in a string of modules (or cells) determines the current of the entire string. The features of each module are never strictly similar when installing genuine modules in the field. The parameters (Isc, Vco, and Pmpp) typically display statistical distributions, which for Pmpp may take the form of squares if they are the outcome of sorting at the manufacturing process's output. This loss corresponds to 2.10%.
- Ohmic wiring loss: Between the power coming from the modules and the power at the sub-array terminals, the wire circuit's ohmic resistance causes losses corresponding to 0.75%

Considering all the losses listed, we go from a nominal array nominal energy of 149.6MWh to an Array virtual energy at MPPT of 134.8 MWh. [15]

Finally, we analyze all losses related to the inverters used, shown in Figure 60.

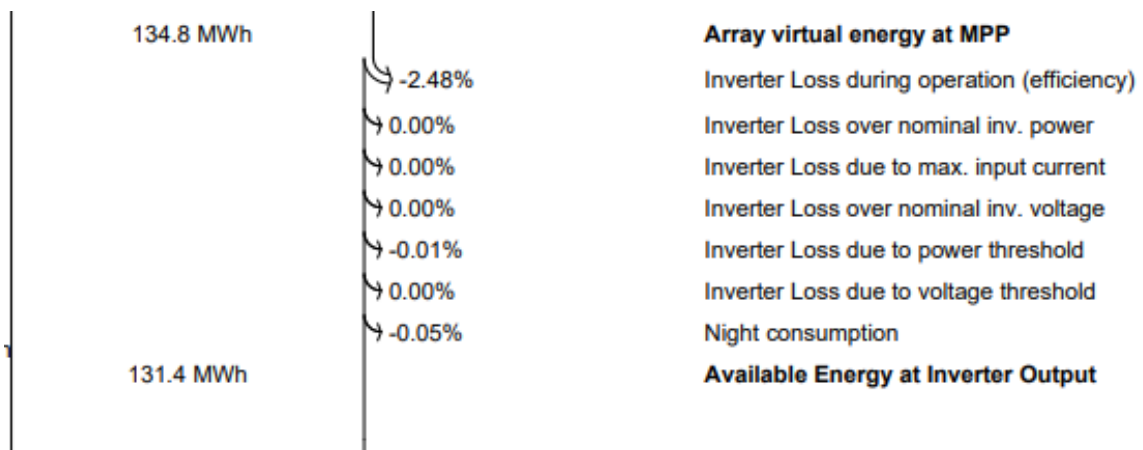


Figura 60: Inverter losses

- Inverter loss during operation: Efficiency of the inverter's DC to AC conversion, adjusted for seasonal variations in power levels, corresponding to 2.48% of the total losses.

The other cause of losses related to inverters are negligible. The diagram of total losses is shown in Figure 61, from which we will then start to discuss the simulation results. As a result of all the losses listed and described above, we obtain a power available at the inverter outputs equal to 131.4MWh.

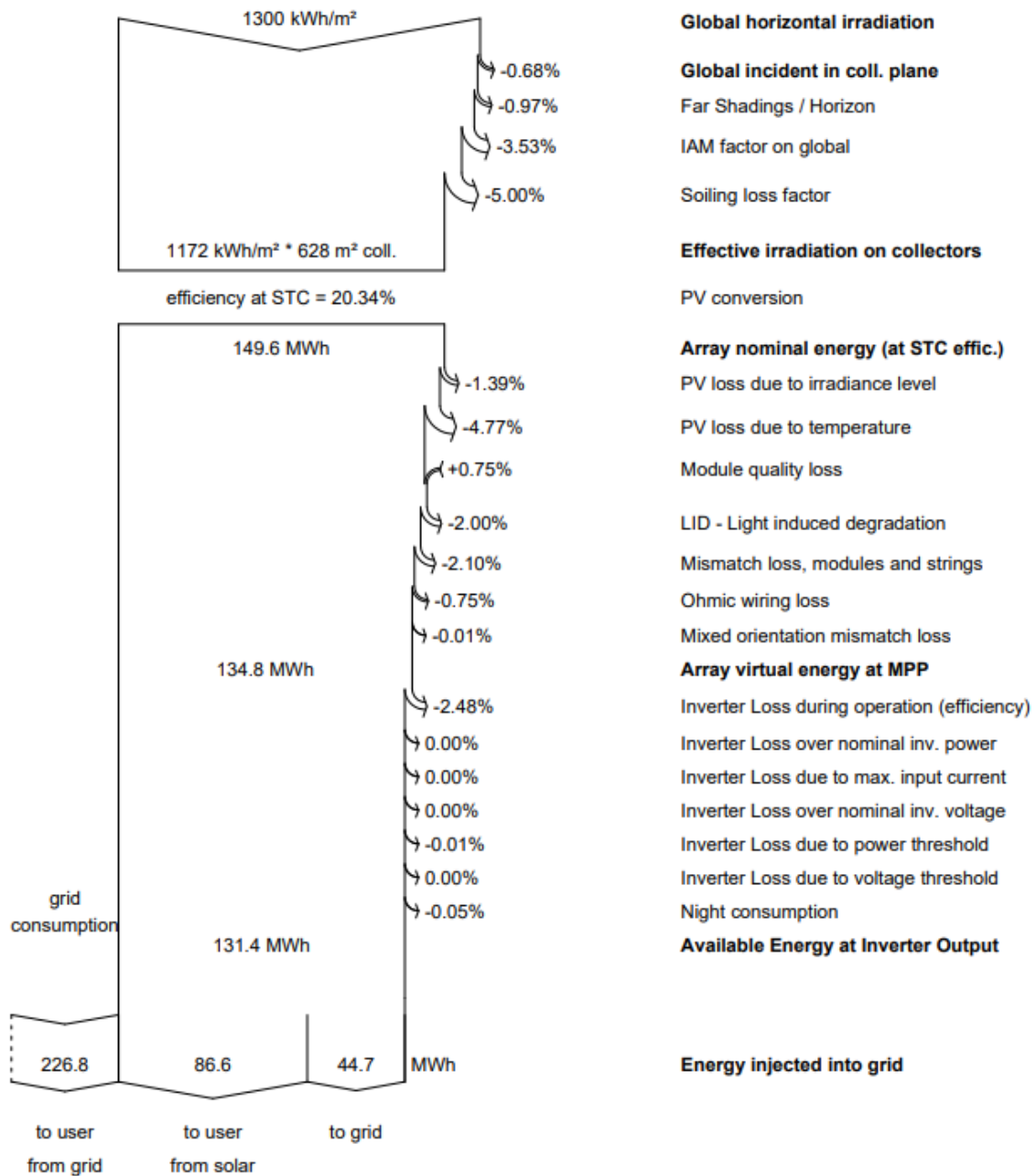


Figura 61: Complete loss diagram

Having analyzed the system in detail and having examined all the causes of losses considered in the simulation, Table 15 summarizes the results obtained for a time of one year, considering the energy consumed by the load seen earlier in the Table 6.

Tabella 15: Main simulation results extrapolated from PVsyst

	GlobHor kWh/m <sup>2</sup>	DiffHor kWh/m <sup>2</sup>	T_Amb °C	GlobInc kWh/m <sup>2</sup>	GlobEff kWh/m <sup>2</sup>	EArray MWh	E_User MWh	E_Solar MWh	E_Grid MWh	EFrGrid MWh
January	37.8	20.63	2.73	37.6	32.2	3.96	44.16	3.82	-0.007	40.35
February	57.3	29.20	4.47	56.9	50.4	6.17	19.90	4.88	1.097	15.02
March	106.7	48.45	9.55	105.9	95.7	11.41	29.08	8.77	2.361	20.31
April	128.6	69.90	13.69	127.5	116.4	13.66	22.22	8.60	4.729	13.61
May	168.9	83.81	18.79	167.6	153.8	17.59	22.67	10.16	7.024	12.51
June	184.4	85.95	23.22	183.3	168.5	18.90	20.99	10.28	8.184	10.71
July	194.8	78.98	25.48	193.9	178.4	19.78	21.73	10.57	8.755	11.16
August	165.1	71.28	24.92	164.0	150.5	16.80	22.60	9.73	6.685	12.87
September	116.3	55.99	19.76	115.5	104.7	12.03	20.96	7.69	4.043	13.27
October	70.1	32.56	14.52	69.7	61.9	7.30	21.15	5.28	1.804	15.87
November	38.4	22.00	8.47	38.0	33.0	3.97	27.89	3.75	0.067	24.15
December	31.4	20.35	3.63	31.1	26.4	3.24	40.09	3.10	-0.008	36.98
Year	1299.8	619.10	14.16	1291.1	1171.8	134.80	313.43	86.64	44.735	226.79

Detailed analysis of the results reveals, as anticipated, that January, February, October, November, and December are the months with the lowest production (E solar) and highest grid purchase (EFrGrid) rates. These are also the months when the least quantity of energy will be injected into the power distribution network because they are the months with the lowest energy production. The software's results indicate that the plant only produces 24.64MWh during these six months, or 18.28% of the energy produced throughout the entire year, which the software assessed to be 134,80kWh (set as 100%) power.

The months of April, May, June, July, and August are those in which the most energy is generated. Estimated production for these months is 86.73 kWh, or 64.3% of the annual average production. The remaining 17,36% of energy generated is dispersed throughout the months of March and September.

As a result of what has been said above, it is evident that the middle months of the year will be those during which more energy is fed into the grid and consequently less energy is absorbed from it. In particular, the following statement can be done:

- During January, February, November and December the energy sold to the grid corresponds to 2,4% of the total energy sold during the year, as a consequence the energy bought from the grid corresponds to 52% of the total energy bought during the year.
- During March and October the energy sold to the grid corresponds to 10% of the total energy sold during the year, as a consequence the energy bought from the grid corresponds to 13,6% of the total energy bought during the year.
- During April, May, June, July and August the energy sold to the grid corresponds to 87,6% of the total energy sold during the year, as a consequence the energy bought from the grid corresponds to 34,4% of the total energy bought during the year.



To conclude, it is interesting to make a further analysis regarding the share of self-consumption and the share of self-sufficiency achieved through the installation of the photovoltaic system. Thus, considering the load consumption along 2021, shown in Table 15, the annual total amounts to 313MWh (E\_User). Considering the total annual output of the installation equals 134.80MWh (E\_Array), of which 86.64MWh were self-consumed (E\_Solar), this results in a self-sufficiency share of 27.68%. While the self-consumption share, equal to the difference between the energy produced and the energy self-consumed is 64.27%. The remaining 35.73% is the share of energy fed into the grid, amounting to 44.73MWh (E\_Grid).

The summary of the results is shown in Figure 62

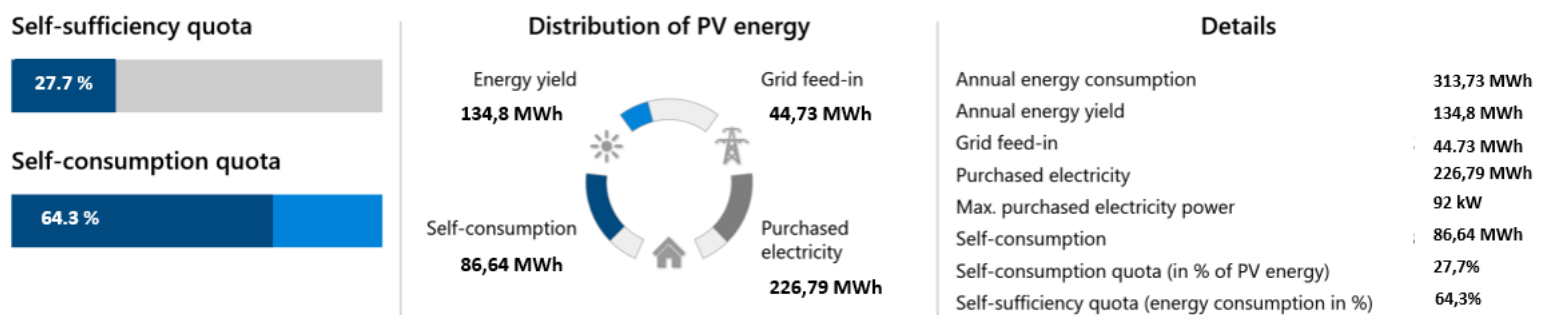


Figura 62:PVsyst results summary

### 2.2.4. Results comparison

Considering the results obtained in the previous chapters, a summary of which is visible in the Table 16.

Tabella 16: SunnyDesign vs. PVsyst results comparison

SunnyDesign vs PVsyst	SunnyDesign	PVsyst
Energy yield	125 MWh	134,8 MWh
Self-consumption	88,010 MWh	86,64 MWh
Grid feed-in	36,771 MWh	44,73 MWh
Purchased electricity	225 MWh	226,79 MWh
Self-consumption quota	70,50%	64,30%
Self-sufficiency quota	28,10%	27,70%

As can be seen, the simulation using SunnyDesign provides a lower total energy produced by the system than the simulation in PVsyst. This is surely due first of all to the fact that PVsyst is able to use the weather data of the specific place of installation of the plant (in the countryside of Piacenza), while SunnyDesign uses solar irradiation data in Milan, where, first and foremost, the greater amount of pollution will make the results less reliable. It can be seen from the comparison table that the share of self-consumed energy is higher in the SunnyDesign simulation than that of PVsyst. The share of self-consumption is higher in SunnyDesign because in the software the actual monthly load consumption could not be defined but was automatically spread out over the course of the year. As a result, in the middle months of the year, the energy demanded by the load is higher than the actual energy demanded, and therefore, since these are the months of highest plant producibility, the share of self-consumed energy increases compared to the PVsyst software. This factor also makes the latter simulation more realistic than SunnyDesign, although worse from the point of view of consumption of energy produced. Since, however, the energy produced by the system is higher and the share of this energy consumed is lower, PVsyst's results show how the excess energy is reflected in a higher share of energy fed into the grid.

As we have already seen, the most reliable simulation is the one performed by PVsyst, because it allows for the correct sizing of all DC and AC cables used in the system, uses

the most accurate weather data, and allows for accurate consideration of all losses analyzed in detail in subsection 2.2.3.2.

At this point the data obtained from the POD installed on site are shown in the Table 17 with the green color. As can be seen, the data in green represent the actual data, corresponding to the first two month of 2023. Unfortunately, as the plant was turned on in January, only data from the first two months of operation are available. Making a comparison with the results obtained from the simulation in PVsyst, it is appreciable to observe that the results are very similar, and the delta between them are in the order of 5%.

Tabella 17: POD + PVsyst final results

Month	Earray [MWh]	E_User [MWh]	E_Solar [MWh]	E_Grid [MWh]	EFrGrid [MWh]
January	3,75	44,16	3,617	0	40,54
February	5,9	19,9	4,66	1,042	15,24
March	11,41	29,08	8,77	2,361	20,31
April	13,66	22,22	8,6	4,729	13,62
May	17,59	22,67	10,16	7,024	12,51
June	18,9	20,99	10,28	8,184	10,71
July	19,78	21,73	10,57	8,755	11,16
August	16,8	22,6	9,73	6,685	12,87
September	12,03	20,96	7,79	4,043	13,17
October	7,3	21,15	5,28	1,804	15,87
November	3,97	27,89	3,75	0,067	24,15
December	3,24	40,09	3,1	-0,008	36,98
Year	134,33	313,44	86,307	44,686	227,13

In Table 18 it is shown the difference between the simulation and the POD's data.

Tabella 18: POD vs PVsyst results

Total of January and February POD vs PVsyst					
Item	Earray [MWh]	E_User [MWh]	E_Solar [MWh]	E_Grid [MWh]	EFrGrid [MWh]
POD	9,65	64,06	8,277	1,042	55,783
PVsyst	10,13	64,06	8,7	1,09	55,37
Delta	4,74%	0,00%	4,86%	4,40%	-0,75%

Regarding the total energy produced by the plant and the actual used solar energy by the load, it is observable in the table that the difference between the simulation and the POD is around 5%, that is an acceptable result.

Given the subtle difference in the results obtained, to enable detailed economic analysis, it was decided to use actual data for the months in which they are available (January and February), while for the remaining months it was decided to consider data obtained from PVsyst. To conclude, a summary of the results obtained by cross-referencing the POD of the Verdeto plant and the simulation performed in PVsyst is shown in the Figure 63.

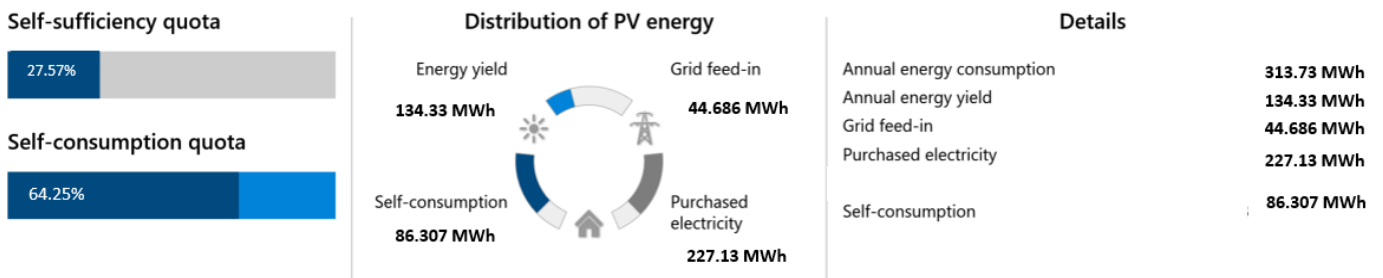


Figura 63: Photovoltaic power plant Verdeto final results

As a result of the intersection of the POD data and the simulation data, we can calculate that the plant produces 134.33MWh of energy, whilst the load actually uses 86.307MWh. As a result, the Self-Consumption Quota is 64.25%. The load has a total energy requirement of 313.73MWh, hence the self-sufficiency quota is 27.57%. In the end, 227.13MWh of energy was bought from the grid over the year. The Verdeto photovoltaic power plant's economic summary will be calculated using these data as an input.

## 3 Economic Overview

### 3.1. Economic Computation

To calculate the investment costs of the plant under consideration, the fixed costs listed in Table 19 were first considered.

Tabella 19: Fixed costs of Verdeto power plant

<b>CAPEX</b>			
<b>Material</b>	<b>Nr.</b>	<b>Cost/unit [€]</b>	<b>Total cost [€]</b>
JA Solar JAM60S20 / MR 380 Wp Mono	336	114,00	38304
SMA inverter Sunny Tripower CORE 1, STP 50-40	3	3415,37	10246,11
SMA DC overvoltage arrester Type II for Core 1	3	48,42	145,26
SMA AC overvoltage arrester Type II for Core 1	3	25,26	75,78
Warranty extension "Active" SMA_Core 1 (STP 50-40)	3	522,09	1566,27
Mounting System PMT Evolution East-West 10°	336	31,88	10711,68
Paving slab made of cement 40x40x4, 15.00 kg	104	1,38	143,52
Bautenschutzmatte KRAITEC TOP 8x1150x2300mm	2	19,48	38,96
blue Log XC-200 Datalogger (532020)	1	508,41	508,41
Radiation sensor Si-V-010-T + 30m cabel (423044)	2	351,46	702,92
Power supply, fixed voltage FPPS 24-27W 24 V/DC	1	21,72	21,72
LANCOM 1790VA-4G+ VDSL Router	1	588,93	588,93
RITTAL Kunststoff-Schaltschrank AX 1434.000	1	97,23	97,23
Transport	1	1105,23	1105,23
Transport substructure_Roof system	1	315,78	315,78
			<b>64571,8</b>

The costs in the above table are for the 336 modules, the 3 inverters, the 3 AC and DC switches of the inverters, the warranty, the PMT substructure, the weights to ballast

the substructures, the data logger, the two irradiation sensors, the router for communication and monitoring of the system with other devices, and finally the transportation of all components. The CAPEX for these components is 64571.8€, not including any margin applied.

In addition to the fixed costs described above, one must consider the cost of installing the company ProEnergy Srl, which was subcontracted for the work. The CAPEX associated with this activity is 39680€ and is inclusive of:

- Safety equipment: temporary safety equipment according to on-site conditions and local standards
- Lifting of equipment: according to on-site conditions and local standards; crane, forklift and/or inclined elevator
- Installation of substructure incl. screen mats, ballast
- Earthing of substructure
- DC cabling from modules to inverters
- Installation of photovoltaic modules and inverters
- Installation of BlueLog , radiation sensor and connection test via GSM Modem
- AC-cabling: inverter to grid connection point ( according to Local Technical Standard) Note: Cable: ARG16R16 3(1X240)+1G95 mmq
- Installation of AC braker on exchange energy meter.
- Administrative works: contents all necessary services which are needed for the planning and permission of PV system at local administrations ( power supply company, supervisory authority, building authority) on the part of EPC;
- Delivery and installation distribution boxes including DC overvoltage protection and safety switch for fire department
- Installation of display and wall bracket
- AC-cabling of display and integrated PC with 220 V
- Data cabling of integrated PC with Lancom Router
- Data cabling of Lidl meters with Weblog

At this point the total fixed costs of the plant amount to 104252€ to which 19% margin of is added to cover all engineering costs practiced by STEAG Sens Italy. The final price of the turnkey plant amounts, with a small discount, to 124000€, and this corresponds to the initial investment.

Following the calculation of the initial investment cost for the turnkey plant, it is necessary to consider the operating and management costs that are present over the entire life of the plant. Table exhibit 20 shows the items that contribute to this.

Tabella 20: Yearly costs of Verdeto Power Plant

OPEX		
Material	Cost	Total cost [€/Year]
Substructures	0,005 [€/Wp]	643,35
WiFi connection	500 [€/year ]	500
Security services	1000 [€/year]	1000
Cleaning service	3000 [€/year]	3000
	<b>Total</b>	<b>5143,35</b>

The costs to be incurred annually are mainly from substructure maintenance, wi-fi connection needed for communication between the plant and external devices, security services, and plant cleaning services. These costs amount to 5143.5€ per year. For economic evaluation, the present value (NPV) and internal rate of return (IRR) were calculated. [16]

$$NPV = -I + \sum_{t=1}^n \frac{B_t}{(1+i)^t} \tag{21}$$

Where in Equation 20:

$I$ =initial investment;

$n$ =duration of the investment project, in this case 10 years;

$i$ =opportunity cost of capital.

$B_t$ =cash flow at year t-th;

The initial investment is what results from the CAPEX calculation. In this case we have assumed as the opportunity cost of capital the weighted average cost of capital, known by the acronym WACC (Weighted Average Cost of Capital). WACC is a weighted average of the cost of equity capital and the cost of debt capital. In the specific case of Verdeto, the plant is financed only with equity capital. So, WACC corresponds to the cost of equity capital  $K_e$ , as can be seen in equation 22. [15]

$$WACC = K_e \tag{22}$$

In this specific case,  $K_e$  is considered at 6% for medium-sized PV systems installed on industrial buildings. [17]

The energy sales price, which was expected to be 100 €/MWh with an annual increase of 1%, was used to compute cash flows over a period of ten years. In addition, an

inflation value of 1% was assumed. Once the NPV has been determined, the investment is valued as follows:

- Accepted if  $NPV > 0$ , because it indicates that the future return is higher than the cost opportunity cost of capital invested
- Rejected if  $NPV < 0$ , because the future return is less than the opportunity cost of the invested capital

The Internal Rate of Return (IRR) is the discount rate that makes the net present value of the cash flows generated by an investment project zero. The equation is the same as that for the NPV, where the NPV takes a value of zero and the unknown becomes precisely the discount rate  $i$ .

$$0 = -I + \sum_{t=1}^n \frac{B_t}{(1+i)^t} \quad (23)$$

The internal rate of return (IRR), which is determined by Equation 23, expresses the return on an investment, i.e., the maximum cost of capital as long as the business is economically viable. When the IRR exceeds the WACC, the project's return surpasses the relative cost of financing, and additional wealth is created. The project implementation would result in financing expenses that could not be offset by the fluxes afterwards generated if the IRR was lower than the WACC. As a result, the investment in the latter scenario should be avoided. The basic data required by both methods of evaluating an investment (NPV and IRR) is the investment's positive and negative cash outflows.

The payback time, also known as the payback time (PBT), which is the length of time needed to recoup an investment, is another factor that is taken into account when analysing an investment. It is thought that the higher the PBT, the greater the risk associated with the investment; nevertheless, picking an investment only based on PBT can negatively impact the lifespan of the project because it disregards its profitability.

Finally, a self-consumption tariff is considered, which is equivalent to the savings one has in the bill due to the self-consumption of energy produced by the system, of 0.25€/kWh, with an evolution of the tariff equivalent to +2% each year.

At this point, the calculation of the NPV, the amortization of the initial investment (equivalent to 124000 euros of equity) and the PBT is shown in Table 21.



Tabella 21: Economic computation

Year	Electricity sale [€]	Run. Costs [€]	Consumption tariff [€/kWh]	Self-cons. Savings [€]	NPV [€]	cumul. Profit [€]	ammort. [%]
2022	4486	5143,35	0,25	21576,75	19735,28	-104264,72	15,92
2023	4549	5148,49	0,26	22008,29	19053,75	-85210,97	31,28
2024	4567	5153,64	0,26	22448,45	18355,60	-66855,37	46,08
2025	4585	5158,80	0,27	22897,42	17682,40	-49172,97	60,34
2026	4603	5163,95	0,27	23355,37	17033,31	-32139,66	74,08
2027	4621	5169,12	0,28	23822,48	16407,50	-15732,16	87,31
2028	4640	5174,29	0,28	24298,92	15804,84	72,69	100,06
2029	4658	5179,46	0,29	24784,90	15223,18	15295,87	112,34
2030	4676	5184,64	0,29	25280,60	14662,49	29958,35	124,16
2031	4694	5189,83	0,30	25786,21	14122,02	44080,38	135,55

Let's examine in greater depth. Table 21:

- The "Electricity sale" column represents the annual injection of 44.686 MWh of electricity into the grid, multiplied by the cost of energy.
- The OPEX is represented by the "Running costs" column.
- The gain resulting from the energy produced by the plant and consumed by the load (86.307MWh) multiplied by the self-consumption tariff is represented in the column labelled "Self-consumption savings".
- The "cumulative profit" column is the difference between the invested capital and the NPV
- The "amortization" column is the percentage of return over invested capital

Looking at Table 21, the NPV at the tenth year is equivalent to 168080.38€, with an amortization of 135.55%, which can be translated into a gain of 44080.48€. The pay back time thus results in 7 years. As we saw earlier, since  $NPV > 0$  implies that the future return is higher than the opportunity cost of invested capital. In addition, because the PBT is less than the assumed lifetime of the study (10 years), the investment is worth the initial capital invested.

Finally, calculating the IRR as in Equation 23 results in a discount rate of 12.85%. So, since this is higher than the WACC (taken to be 6%), we have that the project's return surpasses the relative cost of financing, and additional wealth is created.

## 3.2. Project management

This short chapter describes the 5 days of work direction carried out.

Construction of the system started on 11/08/2022, with 4 electricians present on site. The activities performed were: unloading of the material for the photovoltaic system from the truck and 30% completion of the installation of the interface board, for a total of 8 working hours. The activity of the interface board installation is shown in Figure 64



Figura 64: Interface board installation

On 12/08/2022, the second day of work, there were 4 workers at the site. The activities performed were as follows: interface board installation completed, 90% completion of substructure installation (Figure 65 a), 100% completion of ballast placement to stabilize the substructures (Figure 65 a ), and 60% completion of DC cable installation (Figure 65 b ). It took 10 hours of work to complete the activities just listed.



Figura 65: (a) Substructures installation, (b) DC cable installation

On 08/13/2022, corresponding to the third day of work, there were 4 workers on site. During the actual 10 hours of work, the following activities were completed: finished installation of all DC cables and installed 40% of the PV modules, for a total of 134 modules installed, shown in Figure 66.



Figura 66: Modules installation

On the fourth day of work, dated 14/08/2022, work was proceeding on schedule. On that day, with 4 workers on the job, the following activities were carried out in 10 hours of actual work: 100% completed installation of modules and DC electrical cables (Figure 67 a), 80% completion of cable ducts, 60% completion of panel installation for string paralleling, installation and placement of inverters completed (Figure 67 b).



(a)



(b)

Figura 67: (a) 100% of modules installation, (b) inverters installation

On 08/15/2022, the final work for the completion of the facility took place. Seven workers were needed for a total of 10 actual hours of work. The activities performed were as follows: completion of cable ducts , completion of panel installation for string parallel (Figure 68 a), ground plant installation, *Voc* test performed and installation of the two solar meters (Figure 68 b).



(a)



(b)

Figura 68: (a) parallel panel, (b) solar meters installation

As planned, the work was carried out in 5 days, with no additional expenses beyond those budgeted and with weather conditions that were not adverse (temperatures between 27 and 35 degrees). The work site was also cleaned up and dismantled on 08/15/2022.



## Conclusions

The project's main objective is the thorough review of every aspect of a photovoltaic power generation system. It first examined the components of solar energy before describing the phenomenon of solar irradiation and identifying the variables that have the greatest impact on it. Then, photovoltaic cells are a key component of the description of solar energy conversion technology that follows. After studying the fundamental conversion principles used in cells, a detailed description of their structure and various components was given. The first, second, and third photovoltaic generations were then distinguished, with all of their distinctive qualities and characteristics, using the characteristics and structural configuration of photovoltaic modules as a guide. After the aforementioned elements have been carefully investigated, the second crucial component of photovoltaic systems is analyzed: the conversion unit. First, the general characteristics and operating principles have been examined, and then the possible future configurations that can be obtained depending on the system's power output to which they are connected. The theme of solar cables, both DC and AC, with their sizing principles, and finally the devices needed for interface with the national distribution grid, were examined to finalize the analysis of the state of the art.

The second phase of the project focuses on using all the knowledge learned from the first study in a real-world case study. Project Verdeto, a 127.68kWp photovoltaic power generation plant, is the project that was developed and built during the work done at STEAG Sens Italia. The plant was installed at the location of Verdeto, in the immediate vicinity of Piacenza. Verdeto is defined as a medium-sized self-consuming photovoltaic plant. The unique characteristics of this type of plant are examined in the first step of the case study, comparing the European regulation and delving into the specifics of the Italian regulation. The technical decisions that were made during the project's initial planning stage are carefully examined after the plant's typology has been studied. Therefore, the feasibility analysis is the first stage. As a result, the location of the plant is investigated in chapter 2.2.1.1, followed by a mechanical analysis of an industrial building used for agricultural purposes, an analysis of the expected solar irradiance based on local historical data is deepened in subchapter 2.2.1.2, and finally, in the chapter 2.2.1.3, an investigation of the load that the photovoltaic plant will be required to sustain.

Once the main characteristics of the load, listed in Table 6, the availability of solar radiation in Table 5, the type of surface area that can be used for the installation and thus the available area (discussed in subsection 2.2.1.1) have been clarified, the technical choices made are described in detail.

The PV modules used for the Verdeto plant are JA Solar Module 380W Mono PERC (JAM60S20-380/MR), so first-generation monocrystalline modules equipped with half-cell technology with 9 busbars, together with shorter half-cell cells connected internally in two series of strings. The mechanical characteristics are depicted in Figure 38, and the main technical characteristics in Table 7. In subsection 2.2.2.1, through the use of the main module parameters summarized in Table 10, the main string electrical quantities are dimensioned, which are useful for later analysis. The inverters chosen for this photovoltaic generation plant are three Sunny Tripower CORE1 STP 50-40\_01 from SMA TECHNOLOGIES. The electrical characteristics of these machines are listed in Table 11, while the configurations and thus their stringings are listed in Table 12. The correct sizing of the inverters has been computed in subsection 2.2.2.2, in fact all the verifications performed result in "OK". To conclude the plant sizing phase in subsection 2.2.2.3, the solar cables, both AC and DC, were chosen and verified using the basic parameters in Table 13.

After going through the preliminary technical design phase of the plant, simulations of the plant's producibility are analyzed in chapter 2.2.3.1 and chapter 2.2.3.2. Two software programs were used: SunnyDesign and PVSyst. Specifically, the results obtained are collected in Figure 52 and Figure 62, respectively. As it was previously stated, the software that provides the most reliable results is PVSyst, as it allows to accurately define the losses of the system and also considers the solar irradiation data of the precise location where the Verdeto photovoltaic plant was built, unlike the SunnyDesign software. Assuming what has been previously mentioned, the main results obtained through the simulation in PVSyst, considering that the annual load consumption is 313MWh, are: energy produced by the plant of 134.8MWh, energy consumed by the plant 86.64MWh (corresponding to 64.3% share of self-consumption and 27.7% share of self-sufficiency), energy fed into the grid 44.73MWh and finally energy withdrawn from the national distribution grid 226.79MWh. The prior results are collected, and in section 2.2.4, they are contrasted with the information obtained from the POD that was deployed at Verdeto. Although the plant wasn't turned on until late December, the accuracy of the models for January and February can be confirmed. According to discussion done in section 2.2.4 and as seen in Table 18, the simulation reflects the POD values precisely. In particular, the field instrumentation detected that the plant generated 9.95MWh of total power in January and February, 8.277kWh of that power was utilized to feed loads, and 1.042kWh of that power was injected into the grid. In comparison to the simulation's results, a total power output of 10.13MWh, a power consumption of 8.7MWh, and a power fed into the grid of 1.09MWh are computed for the plant. The highest difference found between the two scenarios is



approximately 5%, a delta that is suitable for further research. For the economic evaluation of the plant, data from the POD for the first two months of the year were taken into account, while projected statistics from PVsyst were utilized for the remaining ten.

The economic analysis computed in Chapter 3.1, performed for a plant life of 10 years, has as output three significant indices for the evaluation of the investment: NPV, IRR and the PBT. Thus, considering all that was previously analyzed and all the considerations made in Chapter 3.1, the NPV results in year 10 of 168080.38€, against an initial investment of 124000€, the IRR results 12.85%, against a WACC of 6% and finally the payback time is 7 years.

All the results obtained in the project and summarized in this chapter lead to the conclusion that self-consumption photovoltaic power plants not only allow for a high proportion of self-sufficiency of the industrial buildings they power, thus decreasing the energy drawn from the grid and thus the pollution generated by power generation, but also turn out to be very good investments from an economic point of view.



## Bibliography

- [1] S. S. V. G. K. M MOHIT KUMAR, "DESIGN OF HIGH EFFICIENT SOLAR PANEL WITH TRACKING SYSTEM," SRM Nagar, Kattankulathur- 603 203, 2016.
- [2] C. a. S.G.Bowden, "Photovoltaics Education Website," 2019. [Online]. Available: [www.pveducation.org](http://www.pveducation.org).
- [3] A. M. O. Sánchez, "PV SYSTEM WITH GLOBAL AND DISTRIBUTED MPPT: COMPARISON OF ENERGY EFFICIENCY UNDER DIFFERENT OPERATING CONDITIONS," POLITECNICO DI MILANO, Milan, 2013-2014.
- [4] B. Diego, "ANALISI E PROGETTAZIONE DI UN IMPIANTO FOTOVOLTAICO CONNESSO ALLA RETE," UNIVERSITÀ DEGLI STUDI DI PADOVA, Padova, 2011-2012.
- [5] L. A. Asmar, "Modelling solar radiation for PV optimisation," Ecole des Ponts ParisTech, Paris, 2021.
- [6] A. R. A. F. S. s. Aktarul Islam, "DESIGN AND IMPLEMENTATION OF SOLAR CHARGE.," June 2016. [Online]. Available: <https://fdocuments.us/document/1234linkedin.html?page=1>.
- [7] P. W. Justyna Pastuszak, "Photovoltaic Cell Generations and Current Research Directions," e, Lublin University of Technology, Nadbystrzycka 38 A, Lublin, Poland, 2022.
- [8] P. A. NWOFE, "Deposition and Characterisation of SnS Thin Films for Application in Photovoltaic Solar Cell Devices," Northumbria University, 2013.

- [9] M. Bolognesi, "ORGANIC BULK-HETEROJUNCTION PHOTOVOLTAIC DEVICES: MATERIALS, DEVICE ARCHITECTURES AND INTERFACIAL PROCESSES," UNIVERSITAT ROVIRA I VIRGILI, 2013.
- [10] A. T. Vishakha Singh, "Study and Comparison of various types of Converters used for Solar PV: A Review," G. L. Bajaj Inst. of Technology and Management Greater Noida,, 2018.
- [11] CEI, Guida alla realizzazione di sistemi di generazione fotovoltaica collegati alle reti elettriche di media e bassa tensione, CEI; 3° edizione, 2010.
- [12] A. SACE, "Quaderni di applicazione tecnica N.10 Impianti fotovoltaici," ABB SpA, 2016.
- [13] O. Bottesi, "Studio e Progettazione di Impianti Fotovoltaici e Controllo della Qualità del Servizio," Università degli studi di Padova, Padova, 2009-2010.
- [14] *REALIZZAZIONE DI UN IMPIANTO FOTOVOLTAICO CONNESSO ALLA RETE ELETTRICA DI DISTRIBUZIONE*, 2022.
- [15] C. Cannatà, "Analisi di sensibilità tecnico-economica per impianti fotovoltaici di grande taglia installati a terra," Politecnico di Torino, Torino, 2018/2019.
- [16] A. Cavallera, "Analisi tecnico economica di installazione fotovoltaica su capannone industriale," Politecnico di Torino, Torino, 2017-2018.
- [17] D. d. energia, "Costi di produzione di energia elettrica da fonti rinnovabili," Politecnico di Milano, Milano, 2013.

## List of Figures

Figure 1: Sun's Energy Distribution .....	9
Figura 2: Extra-terrestrial Solar Radiation .....	10
Figura 3: Spectrum of Solar Radiation .....	11
Figura 4: Global Solar Radiation .....	11
Figura 5: (a) Air Mass Definition, (b) Spectral Power Density .....	12
Figura 6: Solar Radiation Composition .....	13
Figura 7: Silicon Crystal Lattice.....	14
Figura 8: Energy Band Model.....	15
Figura 9: (a) P-type Material Example, (b) N-type Material Example.....	16
Figura 10: p-n Junction Graphic Explanation.....	17
Figura 11: Basic Scheme of PV cell.....	18
Figura 12: Equivalent Circuit of a PV Cell.....	18
Figura 13: Typical Bulk Silicon Module Materials .....	21
Figura 14: Darkned Cell and By-pass Diode .....	23
Figura 15: Connection of Strings in Parallel with Bypass and Blocking Diodes.....	23
Figura 16: I-V and P-V Characteristics Curves of a Solar Cell.....	24
Figura 17: (a) I-V Curve dependence on the solar irradiation level, (b) I-V curve dependence on temperature .....	25
Figura 18: (a) P-V curve dependence on solar irradiation level, (b) P-V curve dependence on temperature .....	26
Figura 19: Monocrystalline silicon panel (left) and polycrystalline silicon panel (right) .....	26
Figura 20: Composition of CdTe solar panel.....	27
Figura 21: Composition of CIGS solar panel .....	28
Figura 22: Composition of a-Si solar panel.....	29
Figura 23: Composition of GaAs solar panel .....	30
Figura 24: Composition of OPV solar panel.....	31

Figura 25: Efficiency of a 3kW inverter and European efficiency .....	33
Figura 26: Typical inverter efficiency (0%-100%) and details between 90% and 100% .....	35
Figura 27: Links between modules, parallel switchboard and inverter .....	41
Figura 28: Scheme of general PV plant connected to the grid according to CEI 0-16 .	43
Figura 29: Single-line diagram of the photovoltaic power plant.....	49
Figura 30: Top-down photo of the building .....	50
Figura 31: Roof cover extrapolated from Autocad .....	51
Figura 32: Cabinet connection identification.....	51
Figura 33: Cartesian solar diagram .....	52
Figura 34 : (a) Solar radiation on the horizontal plane; (b) Producibile energy .....	53
Figura 35: (a) 2020 Energy consumption; (b) 2021 Energy consumption.....	54
Figura 36: Energy consumption 2020 vs 2021 .....	55
Figura 37: (a),(b) Consumption distribution in hourly bands .....	55
Figura 38: module technical diagram .....	56
Figura 39: (a) Current- voltage curve; (b) Power-voltage curve; (c) Current-voltage curve .....	57
Figura 40: PMT EVO 2.0 E/W .....	58
Figura 41: Ballast scheme .....	60
Figura 42: Inverter 1 configuration .....	67
Figura 43: Inverter 1 MPPTs configuration .....	68
Figura 44: Inverter 1 sizing check .....	68
Figura 45: Inverter 2 configuration .....	69
Figura 46: Inverter 2 MPPTs configuration .....	69
Figura 47: Inverter 2 sizing verification .....	70
Figura 48: Inverter 3 configuration .....	70
Figura 49: Inverter 3 sizing verification .....	71
Figura 50: SunnyDesign simulation results.....	71
Figura 51: Energy yield per month .....	72
Figura 52: SunnyDesign results summary .....	73
Figura 53: general parameters of the photovoltaic plant.....	74

Figura 54: photovoltaic array characteristics.....	74
Figura 55: Global horizontal irradiation losses .....	75
Figura 56: Horizon profile.....	75
Figura 57: Array losses .....	76
Figura 58: I(U) curves at different temperature .....	77
Figura 59: Warranty graph provided by manufacturer.....	78
Figura 60: Inverter losses.....	78
Figura 61: Complete loss diagram .....	79
Figura 62:PVsyst results summary .....	81
Figura 63: Photovoltaic power plant Verdeto final results .....	84
Figura 64: Interface board installation.....	90
Figura 65: (a) Substructures installation, (b) DC cable installation.....	91
Figura 66: Modules installation.....	91
Figura 67: (a) 100% of modules installation, (b) inverters installation .....	92
Figura 68: (a) parallel panel, (b) solar meters installation .....	92





## List of Tables

Tabella 1: Albedo Coefficients .....	14
Tabella 2: PV system power value that can be connected to the grid .....	43
Tabella 3: Main self-consumption parameters .....	47
Tabella 4: Italy's self-consumption scheme .....	48
Tabella 5: Daily irradiance and Producibile energy value .....	52
Tabella 6: Verdeto's energy consumption .....	54
Tabella 7: Main modules' parameters .....	57
Tabella 8: Main substructure's parameters.....	58
Tabella 9: Main substructure's load parameters.....	59
Tabella 10: Main modules parameters useful for sizing the PV plant.....	61
Tabella 11: Main inverters' characteristics.....	63
Tabella 12: (a) Inverter 1 string configuration; (b) Inverter 2 string configuration; (c) Inverter 3 string configuration .....	63
Tabella 13: Main cables' characteristic .....	65
Tabella 14: Annual results.....	72
Tabella 15: Main simulation results extrapolated from PVsyst.....	80
Tabella 16: SunnyDesign vs. PVsyst results comparison .....	82
Tabella 17: POD + PVsyst final results .....	83
Tabella 18: POD vs PVsyst results .....	83
Tabella 19: Fixed costs of Verdeto power plant .....	85
Tabella 20: Yearly costs of Verdeto Power Plant .....	87
Tabella 21: Economic computation.....	89

